

First Search for Heavy Neutral Leptons with IceCube DeepCore

Dissertation
zur Erlangung des akademischen Grades
doctor rerum naturalium
(Dr. rer. nat.)

im Fach: Physik
Spezialisierung: Experimentalphysik

eingereicht an der
Mathematisch-Naturwissenschaftlichen Fakultät
der Humboldt-Universität zu Berlin

von
Leander Fischer M. Sc.
geboren am 24. Oktober 1992
in Heidelberg

Präsidentin der Humboldt-Universität zu Berlin
Prof. Dr. Julia von Blumenthal

Dekanin der Mathematisch-Naturwissenschaftlichen Fakultät
Prof. Dr. Caren Tischendorf

Copyright Notice

This book is released into the public domain using the CC-BY-4.0 code.

To view a copy of the CC-BY-4.0 code, visit:

<https://creativecommons.org/licenses/by/4.0/>

Colophon

This document was typeset with the help of KOMA-Script and L^AT_EX using the open-source kaobook template class.

The source code of this thesis is available at:

https://github.com/LeanderFischer/phd_thesis

Todo list

Write introduction (RED)	1
highlight a few more neutrino related open questions, to circle back to related to the HNL searches maybe? (YELLOW)	8
add Majorana condition and mention what this means for interactions (LNV of 2) (ORANGE)	9
Discuss lepton number conservation (pure dirac) and lepton number violation (dirac+majorana) (ORANGE)	9
elaborate on Leptogenesis in ν MSM and sterile neutrino DM, or link some papers? (ORANGE)	10
I think here I'd want the extended leptonic EW lagrangien, so I can explain the mass mixing and the interactions it opens up (RED)	10
mention KENU, Belle, L3 in the text and add references (RED)	11
mention PSI, LSND, NA3 in the text and add references (RED)	12
mention the Z boson decay results from DELPHI (because they are strong in Uttau4, too (RED))	12
Say something about atmospheric neutrino flux uncertainties, based on recent JP/Anatoli papers. (YELLOW)	16
say something about matter effect? (ORANGE)	17
say something about mass ordering? (ORANGE)	17
JVS: I would describe simulation sets you produced in past rather than present tense (ORANGE)	23
add/move event views to here? or draw a schematic of these events? (ORANGE)	23
What is the message of these plots? Make it clear in the text and also in the captions. Potentially cut down to one or two and leave the rest or move them to the appendix. (RED)	31
JVS: The build-up of the weight expression is hard to follow without knowing where it's going. It may be better to start with the fact that the importance sampling weight is the ratio of PDFs, then write down each pdf, then drill down into each of the terms (basically, the standard "tell me what you're going to tell me, then tell me, then tell me what you told me" scheme). (RED)	31
add description of what specific set number means (RED)	39
fix design + significant digits to show (ORANGE)	41
maybe show range/prior and then deviation in sigma, or absolute for the ones without prior	41

Contents

Contents	v
1 Introduction	1
2 Standard Model Neutrinos and Beyond	5
2.1 The Standard Model	5
2.1.1 Fundamental Fields	5
2.1.2 Electroweak Symmetry Breaking	6
2.1.3 Fermion Masses	7
2.1.4 Leptonic Weak Interactions after Symmetry Breaking	7
2.2 Beyond the Standard Model	7
2.2.1 Mass Mechanisms	8
2.2.2 Minimal Extensions and the ν MSM	9
2.2.3 Observational Avenues for Right-Handed Neutrinos	10
2.3 Atmospheric Neutrinos as Source of Heavy Neutral Leptons	15
2.3.1 Production of Neutrinos in the Atmosphere	15
2.3.2 Neutrino Oscillations	16
2.3.3 Neutrino Interactions with Nuclei	18
2.3.4 Heavy Neutral Lepton Production and Decay	19
3 Heavy Neutral Lepton Event Generation	23
3.1 Model-Independent Simulation	23
3.1.1 Simplistic Samples	23
3.1.2 Realistic Sample	24
3.2 Model-Dependent Simulation	26
3.2.1 Custom LeptonInjector	26
3.2.2 Sampling Distributions	30
3.2.3 Weighting Scheme	31
3.3 Background Simulation	32
3.3.1 Neutrinos	33
3.3.2 Muons	34
APPENDIX	35
A Heavy Neutral Lepton Event Generation	37
A.1 Model-Independent Simulation Distributions	37
A.2 Model-Dependent Simulation Distributions	38
B Analysis Results	39
B.1 Final Level Simulation Distributions	39
B.2 Treatment of Detector Systematic Uncertainties	39
B.3 Best Fit Nuisance Parameters	41
Bibliography	43

Introduction

1

Write introduction (RED)

The observation of neutrino oscillations has established that neutrinos have non-zero masses. This phenomenon is not explained by the standard model of particle physics, but one viable explanation to this dilemma is the existence of *heavy neutral leptons (HNLs)*, in the form of right-handed neutrinos with masses much larger than the observed neutrino masses (\gg eV). Depending on their mass and coupling to standard model neutrinos, these particles could also play an important role in solving further problems such as baryogenesis or serve as dark matter candidates.

This work presents the first search for HNLs with the IceCube Neutrino Observatory. The standard three flavor neutrino model is extended by adding a fourth GeV-scale mass state and allowing mixing with the tau neutrino through the mixing parameter $|U_{\tau 4}|^2$. The strength of this mixing is tested using atmospheric neutrinos as a source flux. Muon neutrinos that oscillated into tau neutrinos can produce HNLs through neutral current interactions, which then decay back to standard model particles. Both production and decay may produce observable light in the detector, leading to a unique signature of two cascades at low energies.

The measurement is performed through a binned, maximum likelihood fit, comparing the observed data to the expected events from atmospheric neutrinos and HNLs. Three HNL mass values, m_4 , of 0.3 GeV, 0.6 GeV, and 1.0 GeV are tested using ten years of data, collected between 2011 and 2021. The fits constrain the mixing parameter to $|U_{\tau 4}|^2 < 0.19$ ($m_4 = 0.3$ GeV), $|U_{\tau 4}|^2 < 0.36$ ($m_4 = 0.6$ GeV), and $|U_{\tau 4}|^2 < 0.40$ ($m_4 = 1.0$ GeV) at 90 % confidence level. No significant signal of HNLs is observed for any of the tested masses, and the best fit mixing values obtained are consistent with the null hypothesis of no mixing.

Additionally, a thorough investigation of the unique low energy double cascade signature of HNLs in IceCube is performed. A benchmark reconstruction performance is estimated using a well established IceCube reconstruction tool, after optimizing it for low energy double cascade events. The limitations of the detector to observe these events are identified, and their origins are discussed. This first analysis lays the fundamental groundwork for future searches for HNLs in IceCube.

notes for the introduction

- ▶ observation of non-zero neutrino masses indicates likely existence of new physics beyond the standard model
- ▶ multiple SM neutral fermions (right handed) could explain the neutrino masses and their smallness
- ▶ if they are heavy enough to not be produced in oscillations, they are called heavy neutral leptons
- ▶
- ▶ In 1984 the PS191 [G. Bernardi et al., Phys. Lett. B 166, 479 (1986), G. Bernardi et al., Phys. Lett. B 203, 332 (1988)] experiment at CERN

appears to have been the earliest beam dump to report HNL bounds from the direct production and decay.

During my time at desy and in IceCube, I have been involved in several projects, which are not all directly related to the main analysis presented in this thesis. I will give a brief overview of my scientific contributions and how they are related to the main analysis.

In close collaboration with a former colleague (Alex Trettin), we developed a novel method to treat detector uncertainty effects in IceCube, which we documented in a few author paper, and which is now one of the default method to incorporate detector uncertainties in atmospheric neutrino analyses in IceCube. This method will also be used in the main analysis of this thesis and is briefly introduced in Section ??.

Throughout the last years, I was also involved in updating and maintaining the open source analysis framework PISA, which is used in many analyses.

Work related (what is my original work):

- ▶ the model independent simulation chain described in Section 3.1 was developed exclusively by myself
- ▶ for the model dependent generator presented in Section ??, the skeletal structure was constructed by collaborators, before I took over and implemented the full model dependent simulation chain, including the correct decay widths calculations, custom cross-section, and the weighting scheme, continuously optimizing and testing it, before producing and processing the full samples for the main analysis
- ▶ both the study on how well IceCube can detect low energy double cascades in Chapter ?? and the main analysis in Chapter ?? were developed and performed by myself independently and are original work

[1]: Pauli (1978), "Dear radioactive ladies and gentlemen"

[2]: Cowan et al. (1956), "Detection of the Free Neutrino: a Confirmation"

[3]: Danby et al. (1962), "Observation of High-Energy Neutrino Reactions and the Existence of Two Kinds of Neutrinos"

[4]: Kodama et al. (2001), "Observation of tau neutrino interactions"

[5]: Davis et al. (1968), "Search for Neutrinos from the Sun"

The neutrino was postulated by Wolfgang Pauli [1] in 1930 to explain the continuous energy spectrum of electrons originating from beta decay. Cowan and Reines confirmed this prediction of a light, neutral particle in 1956 when they discovered the electron neutrino using inverse beta decay [2]. Two additional neutrino flavors were found in the following years, and with the discovery of the muon neutrino in 1962 [3] and the tau neutrino in 2001 [4], the current theory of neutrinos in the standard model (SM) was established.

Although neutrinos were first believed to be massless, experimental evidence showing the existence of mixed neutrino states started to appear in the 1960s [5]. Mixing between different physical representations of neutrinos is proof for differences in their masses. The resulting phenomenon of neutrino oscillations can be incorporated into the standard model by extending it to include massive neutrinos. How massive they are and how strong is the mixing between neutrino states has to be obtained from measurement. Today there are a variety of precision oscillation experiments using solar, reactor and atmospheric neutrinos to tighten the constraints on the neutrino oscillation parameters. IceCube is one of those leading experiments probing the oscillation theory with atmospheric neutrinos.

[6]: Aartsen et al. (2017), "The IceCube Neutrino Observatory: instrumentation and online systems"

The IceCube Neutrino Observatory [6] was constructed between 2004 and 2010 at the geographic South Pole. It is the first cubic kilometer Cherenkov

neutrino detector and consists of 5160 optical sensors attached to 86 strings, drilled down to a maximum depth of ~ 2500 m into the Antarctic ice. Neutrinos are detected by the Cherenkov light that is emitted by secondary particles produced in neutrino-nucleon scattering interactions in the ice. With DeepCore, a more densely instrumented sub-array of IceCube, the neutrino detection energy threshold can be lowered to approximately 5 GeV.

At these energies, the similarity in event signatures poses difficulties in identifying different neutrino flavor interactions. Muon neutrino charged-current interactions produce light tracks as opposed to charged-current interactions of electron and tau neutrinos as well as neutral-current interactions of all neutrinos that produce light cascades. The sparse instrumentation of IceCube makes it more challenging to separate track- and cascade-like events. In this thesis, a novel method to distinguish those two event types is developed. In contrast to previously used univariate separation techniques, the multivariate machine learning method applied here maximizes the use of information from the detector response. Through the use of a Gradient Tree Boosting algorithm the separation of events in track and cascade is improved. As a result of the improved separation, the uncertainty to the atmospheric neutrino oscillation parameters Δm_{32}^2 and θ_{23} is significantly reduced.

Standard Model Neutrinos and Beyond

2

2.1 The Standard Model

The SM of particle physics is a Yang-Mills theory [7] providing very accurate predictions of weak, strong, and *electromagnetic* (EM) interactions. It is a relativistic quantum field theory that relies on gauge invariance, where all matter is made up of fermions, which are divided into quarks and leptons, and bosons describe the interactions between the fermions that have to fulfil the overall symmetry of the theory. Leptons are excitations of Dirac-type fermion fields.

The initial idea of the theory is associated with the works of Weinberg [8], Glashow [9], and Salam [10], that proposed a unified description of EM and weak interactions as a theory of a spontaneously broken $SU(2) \times U(1)$ symmetry for leptons, predicting a neutral massive vector boson Z^0 , a massive charged vector boson W^\pm , and a massless photon γ as the gauge bosons. The Higgs mechanism [11], describing the breaking of the symmetry, predicts the existence of an additional scalar particle, the Higgs boson, giving the W^\pm and Z^0 bosons their mass. The Higgs boson was discovered in 2012 at the LHC [12, 13].

Gell-Mann and Zweig proposed the quark model in 1964 [14, 15], which was completed by the discovery of non-abelian gauge theories [16] to form the $SU(3)$ symmetry of the strong interaction called *quantum chromodynamics* (QCD). QCD describes the interaction between quarks and gluons which completed the full picture of the SM in the mid-1970s. Together with the electroweak theory, the SM is a $SU(3)_C \times SU(2)_L \times U(1)_Y$ local gauge symmetry, with the conserved quantities *color* (C), *left-handed chirality* (L), and *weak hypercharge* (Y).

In the following, the basic properties of the SM are described, following the derivations of [17, 18].

2.1.1 Fundamental Fields

Fermions in the SM are Weyl fields with either *left-handed* (LH) or *right-handed* (RH) chirality, meaning they are eigenvectors of the chirality operator γ_5 with $\gamma_5 \psi_{R/L} = \pm \psi_{R/L}$. Only LH particles transform under $SU(2)_L$. The Higgs field is a complex scalar field, a doublet of $SU(2)_L$, which is responsible for the spontaneous symmetry breaking of $SU(2)_L \times U(1)_Y$ to $U(1)_{\text{EM}}$. Local gauge transformations of the fields are given by

$$\psi \rightarrow e^{ig\theta^a(x)T^a} \psi , \quad (2.1)$$

where g is the coupling constant, $\theta^a(x)$ are the parameters of the transformation, and T^a are the generators of the group, with a counting them. The number of bosons is dependent on the generators of the symmetry groups, while the strength is defined by the coupling constants. There are eight massless gluons corresponding to the generators of the $SU(3)_C$ group. These

2.1 The Standard Model	5
2.2 Beyond the Standard Model	7
2.3 Atmospheric Neutrinos as Source of Heavy Neutral Leptons	15

[7]: Yang et al. (1954), "Conservation of Isotopic Spin and Isotopic Gauge Invariance"

[8]: Weinberg (1967), "A Model of Leptons"

[9]: Glashow (1961), "Partial-symmetries of weak interactions"

[11]: Higgs (1964), "Broken symmetries, massless particles and gauge fields"

[12]: Chatrchyan et al. (2012), "Observation of a New Boson at a Mass of 125 GeV with the CMS Experiment at the LHC"

[13]: Aad et al. (2012), "Observation of a new particle in the search for the Standard Model Higgs boson with the ATLAS detector at the LHC"

[14]: Gell-Mann (1964), "A Schematic Model of Baryons and Mesons"

[15]: Zweig (1964), "An $SU(3)$ model for strong interaction symmetry and its breaking. Version 2"

[17]: Giunti et al. (2007), *Fundamentals of Neutrino Physics and Astrophysics*

[18]: Schwartz (2013), *Quantum Field Theory and the Standard Model*

mediate the strong force which conserves color charge. The W_1, W_2, W_3 , and B boson fields of the $SU(2)_L \times U(1)_Y$ group are mixed into the massive bosons through spontaneous symmetry breaking as

$$W^\pm = \frac{1}{\sqrt{2}}(W_1 \mp iW_2) \quad (2.2)$$

and

$$Z^0 = \cos \theta_W W_3 - \sin \theta_W B, \quad (2.3)$$

with θ_W being the *Weinberg angle*. The massless photon field is given by

$$A = \sin \theta_W W_3 + \cos \theta_W B \quad (2.4)$$

and its conserved quantity is the EM charge Q , which depends on the weak hypercharge, Y , and the third component of the weak isospin, T_3 , as $Q = T_3 + Y/2$.

	Type			Q
quarks	u	c	t	+2/3
	d	s	b	-1/3
leptons	ν_e	ν_μ	ν_τ	0
	e	μ	τ	-1

Table 2.1: Fermions in the Standard Model. Shown are all three generations of quarks and leptons with their electric charge Q .

Fermions are divided into six quarks and six leptons, which are listed in Table 2.1. The quarks interact via the weak, the strong, and the EM force, and they are always found in bound form as baryons or mesons. Leptons do not participate in the strong interaction and only the electrically charged leptons are massive and are effected by the EM force, while neutrinos are massless and only interact via the weak force. Each charged lepton has an associated neutrino, which it interacts with in *charged-current (CC)* weak interactions, that will be explained in more detail in Section 2.1.4.

2.1.2 Electroweak Symmetry Breaking

To elaborate the process of spontaneous symmetry breaking through which the gauge bosons of the weak interaction acquire their masses, the Lagrangian of the Higgs field is considered as

$$\mathcal{L}_{\text{Higgs}} = (D_\mu \Phi^\dagger)(D^\mu \Phi) - \lambda \left(\Phi^\dagger \Phi - \frac{v^2}{2} \right)^2, \quad (2.5)$$

with parameters λ and v , where λ is assumed to be positive. Φ is the Higgs doublet, which is defined as

$$\Phi = \begin{pmatrix} \Phi^+ \\ \Phi^0 \end{pmatrix}, \quad (2.6)$$

with the charged component Φ^+ and the neutral component Φ^0 . The covariant derivative is given by

$$D_\mu = \partial_\mu - ig_2 \frac{\sigma^i}{2} W_\mu^i - \frac{1}{2}ig_1 B_\mu, \quad (2.7)$$

with the Pauli matrices σ^i and the gauge boson fields W_μ^i and B_μ of the $SU(2)_L$ and $U(1)_Y$ groups, respectively. The coupling constants g_2 and g_1 are the respective coupling constants which are related to the Weinberg angle as $\tan \theta_W = \frac{g_1}{g_2}$. The Higgs potential has a non-zero *vacuum expectation value (vev)* at the minimum of the potential at $\Phi^\dagger \Phi = \frac{v^2}{2}$. Since the vacuum is electrically neutral, it can only come from a neutral component of the Higgs

doublet as

$$\Phi_{\text{vev}} = \frac{1}{\sqrt{2}} \begin{pmatrix} 0 \\ v \end{pmatrix}. \quad (2.8)$$

2.1.3 Fermion Masses

The mass term for charged fermions with spin-1/2 is given by

$$\mathcal{L}_{\text{Dirac}} = m(\bar{\Psi}_R \Psi_L - \bar{\Psi}_L \Psi_R), \quad (2.9)$$

composed of the product of LH and RH Weyl spinors $\Psi_{L/R}$. This term is not invariant under $SU(2)_L \times U(1)_Y$ gauge transformations, but adding a Yukawa term

$$\mathcal{L}_{\text{Yukawa}} = -Y^e \bar{L}_L \Phi e_R + h.c., \quad (2.10)$$

coupling the fermion fields e_R to the Higgs field Φ , recovers the invariance and gives the fermions their masses. Here, Y^e is the Yukawa coupling constant and \bar{L}_L is the $SU(2)_L$ doublet. With the vev, this results in the mass term for the charged leptons and down-type quarks of $-m_e(\bar{e}_L e_R + \bar{e}_R e_L)$ with $m_e = \frac{Y^e v}{\sqrt{2}}$. With $\tilde{\Phi} = i\sigma_2 \Phi^*$, a similar Yukawa term can be written as $-Y^u \bar{L}_L \tilde{\Phi} u_R + h.c.$, which leads to the masses of the up-type quark fields u_R .

2.1.4 Leptonic Weak Interactions after Symmetry Breaking

After the spontaneous symmetry breaking, the leptonic part of the electroweak Lagrangian can be written as

$$\begin{aligned} \mathcal{L}_{\text{EW}}^\ell &= \frac{g}{\sqrt{2}} W^+ \sum_{\alpha=e,\mu,\tau} \bar{\nu}_\alpha \gamma^\mu P_L \ell_\alpha + \frac{g}{4c_w} Z \\ &\times \left\{ \sum_{\alpha=e,\mu,\tau} \bar{\nu}_\alpha \gamma^\mu P_L \nu_\alpha + \sum_\alpha \bar{\ell}_\alpha \gamma^\mu [2s_w^2 P_R - (1 - 2s_w^2) P_L] \ell_\alpha \right\} + h.c., \end{aligned} \quad (2.11)$$

where $c_w \equiv \cos \theta_w$, $s_w \equiv \sin \theta_w$, P_L and P_R are the left and right projectors, respectively, while ν_α and ℓ_α are the neutrino and charged lepton weak eigenstates. The W^+ and Z bosons are the massive gauge bosons of the weak interaction. The large boson masses $m_W \sim 80$ GeV and $m_Z \sim 90$ GeV result in a short range of the force of about 1×10^{-18} m. Interactions carried out by the W^\pm bosons are called *charged current (CC)* interactions, as they propagate a charge, therefore changing the interacting lepton to its charged/neutral counterpart. *Neutral current (NC)* interactions are those mediated by the Z^0 boson, where no charge is transferred. NC interactions couple neutrinos to neutrinos and charged leptons to charged leptons, but not to each other. The Feynman diagrams for CC and NC interactions are shown in Figure 2.1.

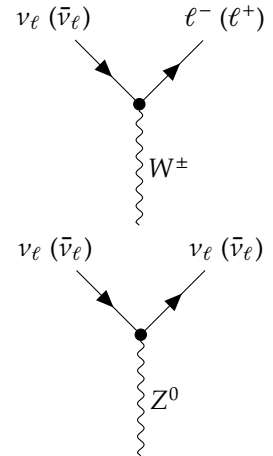


Figure 2.1: Feynman diagrams of charged-current (top) and neutral-current (bottom) neutrino weak interactions, modified from [19].

2.2 Beyond the Standard Model

The fundamentals of the SM described above are **not** enough to explain all observed phenomena. The SM is unable to account for gravity, as it is incompatible with general relativity. Similarly, it fails to explain some cosmological observations like DM, and the matter-antimatter asymmetry

in the universe. But most importantly, the SM does not predict neutrinos to have mass, which on the contrary is experimentally proven by observation of neutrino oscillations, so some extension to the SM is needed to complete the full picture.

[20]: Deruelle et al. (2018), *Relativity in Modern Physics*

[21]: Workman et al. (2022), “Review of Particle Physics”

[22]: Fukugita et al. (1986), “Baryogenesis without grand unification”

[5]: Davis et al. (1968), “Search for Neutrinos from the Sun”

[23]: Fukuda et al. (1998), “Evidence for Oscillation of Atmospheric Neutrinos”

[24]: Ahmad et al. (2002), “Direct Evidence for Neutrino Flavor Transformation from Neutral-Current Interactions in the Sudbury Neutrino Observatory”

[25]: Alam et al. (2021), “Completed SDSS-IV extended Baryon Oscillation Spectroscopic Survey: Cosmological implications from two decades of spectroscopic surveys at the Apache Point Observatory”

[26]: Aghanim et al. (2020), “Planck2018 results: VI. Cosmological parameters”

[27]: Aker et al. (2022), “Direct neutrino-mass measurement with sub-electronvolt sensitivity”

highlight a few more neutrino related open questions, to circle back to related to the HNL searches maybe? (YELLOW)

The standard cosmological model Λ CDM [20] assumes that equal amounts of matter and anti-matter were produced in the early universe. However, the universe today is dominantly made up of matter. This BAU can be measured by the difference between the number densities of baryons and anti-baryons normalized to the number density of photons as

$$\eta_B = \frac{n_B - n_{\bar{B}}}{n_\gamma} , \quad (2.12)$$

where n_B , $n_{\bar{B}}$, and n_γ are the number densities of baryons, anti-baryons, and photons, respectively. Baryons are the dominant component with η_B being observed to be at the order of 10^{-9} [21]. Leptogenesis and EW baryogenesis are scenarios that could explain this phenomenon, where the former could be realized by the existence of heavy RH neutrinos [22].

The observation of neutrino flavor conversions and neutrino oscillations in a multitude of experiments [5, 23, 24] is the strongest evidence for physics *beyond the standard model (BSM)* measured in laboratories to date. The observation that neutrinos change their flavor while they propagate through space can only be explained, if at least two neutrinos have a non-zero mass. From those measurements we know the mass differences are very small as compared to the lepton masses, but neither their existence, nor their smallness is predicted by the SM. There are upper limits on the sum of all neutrino masses from cosmological observations at 1.2 eV [25, 26] and at 0.8 eV from the KATRIN experiment [27]. Adding RH neutrino states to the theory could explain the origin of the observed non-zero neutrino masses and could be tested for by searching for corresponding signatures in experiments.

2.2.1 Mass Mechanisms

Since there are no RH neutrinos in the SM, the mass mechanism described in Section 2.1.3, which couples the Higgs field to LH and RH Weyl fields, predicts the LH neutrinos to be massless. From experimental observations it is known that at least two of the three neutrino generations need to have a non-zero mass. Assuming the existence of RH neutrino fields ν_R , one way of producing the neutrino masses is by adding a Yukawa coupling term similar to the one for up-type quarks mentioned in Section 2.1.3, to write the full Yukawa Lagrangian as

$$\mathcal{L}_{\text{Yukawa}} = -Y_e^e \bar{L}_L^i \Phi e_R^j - Y_\nu^v \bar{L}_L^i \tilde{\Phi} \nu_R^j + h.c. , \quad (2.13)$$

with i, j running over the three generations of leptons e, μ , and τ , and Y^e and Y^ν being the Yukawa coupling matrices. Diagonalizing the Yukawa coupling matrices through unitary transformations U^e and U^ν leads to the **Dirac mass term** in the mass basis as

$$\mathcal{L}_{\text{Dirac}}^{\text{mass}} = \frac{v}{\sqrt{2}} (\bar{e}_L M_e e_R - \bar{\nu}_L M_\nu \nu_R) , \quad (2.14)$$

where M_e and M_ν are the diagonal mass matrices of leptons and neutrinos, respectively. A purely Dirac mass term would not explain the smallness of the neutrino masses in a straightforward way. Only fine-tuning the Yukawa coupling constants to small values would lead to small neutrino masses.

An additional way of generating neutrino masses is by adding a Majorana mass term of the form

$$\mathcal{L}_{\text{Majorana}} = -\frac{1}{2} M_{ij} (\nu_R^i)^c \nu_R^j + h.c., \quad (2.15)$$

with M_{ij} being the Majorana mass matrix and the indices i, j running over all n_R RH neutrino generations. The superscript c denotes the charge conjugate field. Combining the charge conjugated RH neutrino fields with the LH neutrino fields as

$$N = \begin{pmatrix} \nu_L \\ \nu_R^c \end{pmatrix}, \quad (2.16)$$

with ν_R containing the n_R RH fields. The full neutrino mass Lagrangian is then given by the combined **Dirac and Majorana mass term** as

$$\mathcal{L}_{\text{Dirac+Majorana}}^{\text{mass},\nu} = \frac{1}{2} N^T \hat{C} M^{D+M} N + h.c., \quad (2.17)$$

and the mass matrix is given by

$$M^{D+M} = \begin{pmatrix} 0 & (M^D)^T \\ M^D & M^R \end{pmatrix}. \quad (2.18)$$

On top of explaining the origin of neutrino masses itself, a combined Dirac and Majorana mass term could also solve the question of their smallness. If the mass of the RH neutrinos is very large, the masses of the active neutrino flavors is suppressed, which is known as *see-saw mechanism*.

add Majorana condition and mention what this means for interactions (LNV of 2) (ORANGE)

2.2.2 Minimal Extensions and the ν MSM

Discuss lepton number conservation (pure dirac) and lepton number violation (dirac+majorana) (ORANGE)

So far we have described neutrinos in their flavor eigenstates, which are relevant for weak interactions, where the three weak flavor states ν_e, ν_μ , and ν_τ are related to the charged leptons they interact with in CC interactions. In order to *just* explain the three oscillating flavor eigenstates, three mass states are needed, which are related to the flavor eigenstates by the unitary, 3×3 Pontecorvo-Maki-Nakagawa-Sakata (PMNS) mixing matrix U , where the flavor states are a superposition of the mass states as

$$|\nu_\alpha\rangle = \sum_k U_{\alpha k}^* |\nu_k\rangle, \quad (2.19)$$

with the weak flavor states $|\nu_\alpha\rangle$, $\alpha = e, \mu, \tau$, and the mass states $|\nu_k\rangle$ with $k = 1, 2, 3$. In its generic form the PMNS matrix is given by

$$U = \begin{pmatrix} U_{e1} & U_{e2} & U_{e3} \\ U_{\mu 1} & U_{\mu 2} & U_{\mu 3} \\ U_{\tau 1} & U_{\tau 2} & U_{\tau 3} \end{pmatrix}, \quad (2.20)$$

which will be the basis for the discussion of neutrino oscillations in Section 2.3.2.

This however is not enough to explain the neutrino masses observed in oscillation experiments. The most minimal model required to give rise to two non-zero active neutrino masses, is an additional two RH neutrinos, assuming the mass of the lightest SM neutrino is zero. If the additional neutrino states have masses \gg eV they are referred to as HNL, which are almost sterile, with a small mass mixing with the active neutrinos.

But the SM also fails to explain additional observations of physics beyond the standard model (BAU, DM), which could be solved by the *neutrino minimal standard model* (ν MSM) [28, 29]. In the ν MSM, three RH neutrinos are added, where two of them are heavy, to explain the observed neutrino masses and oscillations, and a third one is light and serves as a DM candidate. The mixing between mass and flavor eigenstates is then described by an extended 6×6 mixing matrix as

$$\begin{pmatrix} \nu_e \\ \nu_\mu \\ \nu_\tau \\ N_1 \\ N_2 \\ N_3 \end{pmatrix} = \begin{pmatrix} U_{e1} & U_{e2} & U_{e3} & U_{e4} & U_{e5} & U_{e6} \\ U_{\mu 1} & U_{\mu 2} & U_{\mu 3} & U_{\mu 4} & U_{\mu 5} & U_{\mu 6} \\ U_{\tau 1} & U_{\tau 2} & U_{\tau 3} & U_{\tau 4} & U_{\tau 5} & U_{\tau 6} \\ U_{N_1 1} & U_{N_1 2} & U_{N_1 3} & U_{N_1 4} & U_{N_1 5} & U_{N_1 6} \\ U_{N_2 1} & U_{N_2 2} & U_{N_2 3} & U_{N_2 4} & U_{N_2 5} & U_{N_2 6} \\ U_{N_3 1} & U_{N_3 2} & U_{N_3 3} & U_{N_3 4} & U_{N_3 5} & U_{N_3 6} \end{pmatrix} \begin{pmatrix} \nu_1 \\ \nu_2 \\ \nu_3 \\ \nu_4 \\ \nu_5 \\ \nu_6 \end{pmatrix}, \quad (2.21)$$

where N_i and ν_{i+3} ($i \in [1, 2, 3]$) are the sterile flavor states and the additional RH mass states, respectively. In the ν MSM, the two heavy RH neutrinos generate the active neutrino masses through the type I seesaw mechanism [30–34], where they are assumed to be SM scalars and couple to the Higgs field as such.

2.2.3 Observational Avenues for Right-Handed Neutrinos

If the RH neutrinos have masses at the eV scale, they can be observed through distortion effects in measurements of neutrino oscillation experiments. Several analyses looking for these so-called light sterile neutrinos exist in IceCube, where [35] is using atmospheric neutrinos in the higher energy range of 500 GeV to 10 000 GeV and [19] is using the lower energy region of 6 GeV to 156 GeV. The latter work includes a detailed description of the expected oscillation effects and the various anomalies observed in oscillation experiments that could be explained by the existence of a light sterile neutrino, which is not covered in this work.

Here, the focus will be on heavy RH neutrinos, interchangeably also called heavy sterile neutrinos, or HNLs. A defining property is that they are too massive to be produced in oscillations and to be observed as distortions thereof. Several ways to observe HNLs are possible through direct production and decay experiments, which will be discussed in the following. Most of the existing searches assume the minimal model, where only one coupling between the new mass states and the SM neutrinos is non-zero and the coupling is just through mass mixing in a type I seesaw scenario, but more complex scenarios are of course also possible and might produce various additional signatures, or stronger signals.

In general, the constraints discussed in the following are based on models, where only the coupling between the HNL and one SM flavor is non-zero. While this is the straight forward approach to test the mixing parameters individually, this might make the constraints stronger than they would be

[28]: Asaka et al. (2005), "The nuMSM, dark matter and neutrino masses"

[29]: Asaka et al. (2005), "The ν MSM, dark matter and baryon asymmetry of the universe"

elaborate on Leptogenesis in ν MSM and sterile neutrino DM, or link some papers? (ORANGE)

[30]: Minkowski (1977), " $\mu \rightarrow e \gamma$ at a rate of one out of 10^9 muon decays?"

[31]: Yanagida (1980), "Horizontal Symmetry and Masses of Neutrinos"

[32]: Glashow (1980), "The Future of Elementary Particle Physics"

[33]: Gell-Mann et al. (1979), "Complex Spinors and Unified Theories"

[34]: Mohapatra et al. (1980), "Neutrino Mass and Spontaneous Parity Nonconservation"

I think here I'd want the extended leptonic EW lagrangian, so I can explain the mass mixing and the interactions it opens up (RED)

[35]: Aartsen et al. (2020), "eV-Scale Sterile Neutrino Search Using Eight Years of Atmospheric Muon Neutrino Data from the IceCube Neutrino Observatory"

[19]: Trettin (2023), "Search for eV-scale sterile neutrinos with IceCube DeepCore"

in a more complex scenario, where the HNLs couple to more than one SM flavor as was shown in [36] for collider bounds.

Extracted Beamline Searches

[36]: Tastet et al. (2021), “Reinterpreting the ATLAS bounds on heavy neutral leptons in a realistic neutrino oscillation model”

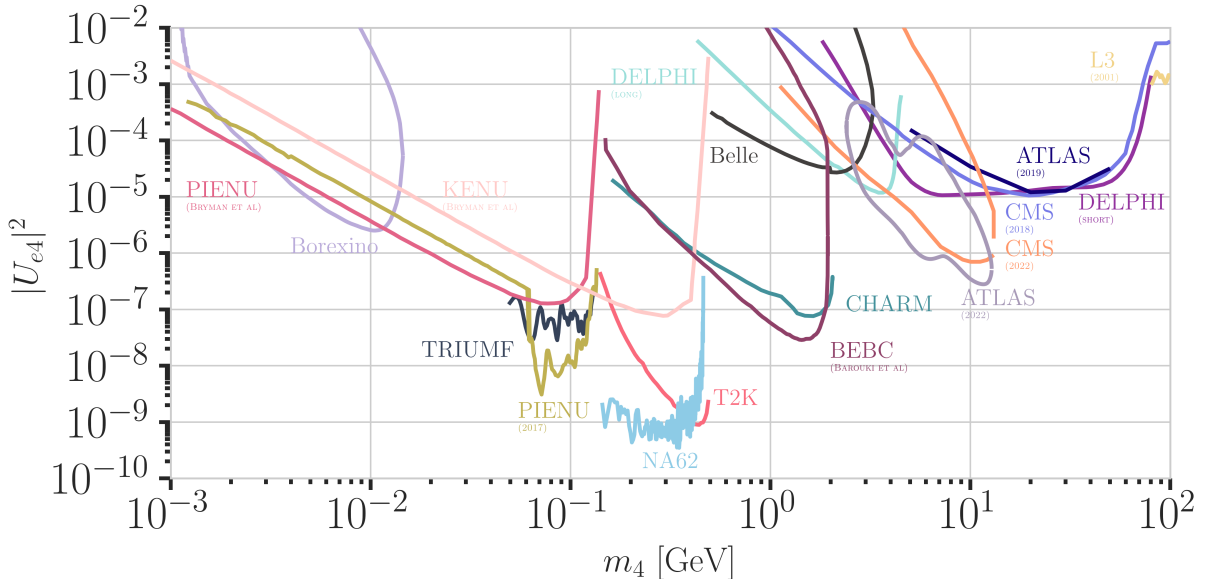


Figure 2.2: Current leading $|U_{e4}|^2 - m_4$ upper limits from PIENU [37, 38], BOREXINO [39], KENU [40], DELPHI [43], BEBC [44], Belle [45], L3 [46], CHARM [47], ATLAS [48, 49], CMS [48, 49], and NuTeV [50]. Modified from [51].

Protons interacting with a target or a beam dump can produce pions, kaons, and heavy-quark hadrons, whose subsequent decays would also produce HNLs. The energies of the HNLs produced in those interactions would be between 1 MeV and 4 GeV and could decay at several distances, depending on their lifetime, which is model dependent. Experiments along the extracted beamline, which are using a spectrometer with particle identification, can search for unique decay signatures at displaced vertices. Example signatures are $\nu_4 \rightarrow l_\alpha \pi$, $\nu_4 \rightarrow l_\alpha^+ l_\alpha^-$, or $\nu_4 \rightarrow \nu \pi^0$ (or other neutral mesons), which cannot be explained by SM neutrinos. Depending on the decay channel, a specific mixing can be probed. The other way of searching for HNLs with these interactions is to look for peaks in the missing mass spectrum, measured around the production vertex at the target, which usually is not possible for beam dumps, as the beam dump region is not calorimetrically instrumented.

HNL search pioneer work was done by experiments at extracted beam lines, with first results from PS191 [52] and CHARM [45], reporting bounds from direct production and decay of HNLs for $|U_{e4}|^2$, $|U_{\mu 4}|^2$, and combinations of them, at masses from 10 MeV to 500 MeV at orders of 10^{-3} to 10^{-6} . Since then, there has been and still is a large activity of searches for HNLs at extracted beamlines and the strongest bounds on $|U_{e4}|^2$ and $|U_{\mu 4}|^2$ are currently set by PIENU [37, 38, 53], TRIUMF [40], NA62 [41], T2K [42], BNL-E949 [54], MicroBooNE [55], and NuTeV [50] in the mass range from 1 MeV to 4 GeV, reaching from 10^{-4} at the lower mass to 10^{-9} at 4 at the highest masses. The current strongest bounds are shown in Figure 2.2 and Figure 2.3, which also shows bounds from other experiments, which will be discussed in the following.

L3 in the text and add references (RED)

[52]: Bernardi et al. (1986), “Search for Neutrino Decay”

[45]: Bergsma et al. (1983), “A Search for Decays of Heavy Neutrinos”

[37]: Bryman et al. (2019), “Constraints on Sterile Neutrinos in the MeV to GeV Mass Range”

[38]: Aguilar-Arevalo et al. (2018), “Improved search for heavy neutrinos in the decay $\pi \rightarrow e\nu$ ”

[53]: Ito et al. (2021), “Search for heavy neutrinos in $\pi^+ \rightarrow \mu^+ \nu$ decay and status of lepton universality test in the PIENU experiment”

[40]: Britton et al. (1992), “Improved search for massive neutrinos in $\pi^+ \rightarrow e + \nu$ decay”

[41]: Parkinson et al. (2022), “Search for heavy neutral lepton production at the NA62 experiment”

[42]: Abe et al. (2019), “Search for heavy neutrinos with the T2K near detector ND280”

[54]: Artamonov et al. (2015), “Search for heavy neutrinos in $K^+ \rightarrow \mu^+ \nu_H$ decays”

[55]: Abratenko et al. (2024), “Search for Heavy Neutral Leptons in Electron-Positron and Neutral-Pion Final States with the MicroBooNE Detector”

[50]: Vaitaitis et al. (1999), “Search for neutral heavy leptons in a high-energy neutrino beam”

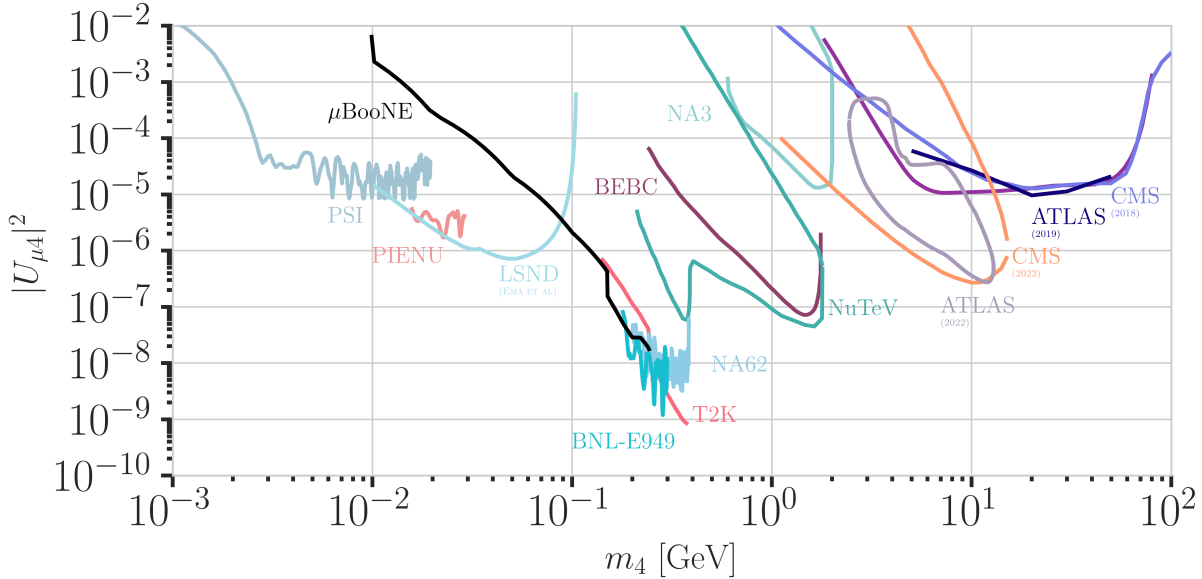


Figure 2.3: Current leading $|U_{\mu 4}^2| - m_4$ upper limits from PSI , μ BooNE [55], PIENU [37], LSND , BNL-E949 [54], NA62 [41], T2K [42], BEBC [59], ATLAS [46, 47], CMS [48, 49], NuTeV [50], and NA3 . Modified from [51].

[56]: Astier et al. (2001), “Search for heavy neutrinos mixing with tau neutrinos”

[44]: Barouki et al. (2022), “Blast from the past II: Constraints on heavy neutral leptons from the BEBC WA66 beam dump experiment”

[57]: Orloff et al. (2002), “Limits on the mixing of tau neutrino to heavy neutrinos”

[58]: Boiarska et al. (2021), “Constraints from the CHARM experiment on heavy neutral leptons with tau mixing”

mention PSI, LSND, NA3 in the text and add references (RED)

[46]: Aad et al. (2019), “Search for heavy neutral leptons in decays of W bosons produced in 13 TeV pp collisions using prompt and displaced signatures with the ATLAS detector”

[47]: Aad et al. (2023), “Search for Heavy Neutral Leptons in Decays of W Bosons Using a Dilepton Displaced Vertex in $\sqrt{s} = 13$ TeV pp Collisions with the ATLAS Detector”

[48]: Sirunyan et al. (2018), “Search for heavy neutral leptons in events with three charged leptons in proton-proton collisions at $\sqrt{s} = 13$ TeV”

[49]: Tumasyan et al. (2022), “Search for long-lived heavy neutral leptons with displaced vertices in proton-proton collisions at $\sqrt{s} = 13$ TeV”

[60]: Shuve et al. (2016), “Revision of the LHCb Limit on Majorana Neutrinos”

Especially noteworthy are the results of analyses probing the mixing with the third lepton generation, $|U_{\tau 4}|^2$, from NOMAD [56] and reinterpretations of the CHARM results and the BEBC results in the context of the mixing $|U_{\tau 4}|^2$, where the latter places the most stringent limits from 10^{-3} to 10^{-6} in the 0.1 GeV to 2 GeV range [44, 57, 58]. In Figure 2.4 the current strongest bounds on $|U_{\tau 4}|^2$ are shown.

Collider Searches

So far, collider searches have been conducted at the *large electron positron collider* (LEP) and at the *large hadron collider* (LHC) in proton-proton mode. Strongest results are from the ATLAS and CMS experiments, which are nearly hermetic, general purpose detectors around the interaction point, and from the *DELPHI* and the *LHCb* experiments, which are forward detectors that can be used to search for new particles in decays of heavy particles produced. In the minimal model, HNLs in the GeV mass range can be produced through mass mixing in decays of heavy mesons, tau leptons, Z/W bosons, H bosons, or top quarks originating from the collisions. Depending on the dirac or majorana nature of the HNL, they can decay to lepton number conserving or lepton number violating channels.

Using prompt and displaced decays of the HNL, both ATLAS and CMS have set constraints on $|U_{e 4}|^2$ and $|U_{\mu 4}|^2$ at the level of 10^{-4} to 10^{-6} in the mass range between 1 GeV to 100 GeV [46–49]. The LHCb experiment has HNL search results at HNL masses below and above the W boson mass, where the low mass searches are using the decay channel $B^- \rightarrow \pi^+ \mu^- \mu^-$, setting limits at the 10^{-3} level for $|U_{\mu 4}|^2$ in the mass range of 0.5 GeV to 3.5 GeV [60]. At high masses, the $W^+ \rightarrow \mu^- \mu^\pm$ jet channel is used to set limits at the order of 10^{-3} to 10^{-2} for $|U_{\mu 4}|^2$ in the mass range of 5 GeV to 50 GeV in the LNC channel and at the order of 10^{-4} to 10^{-3} in the LNV channel [61].

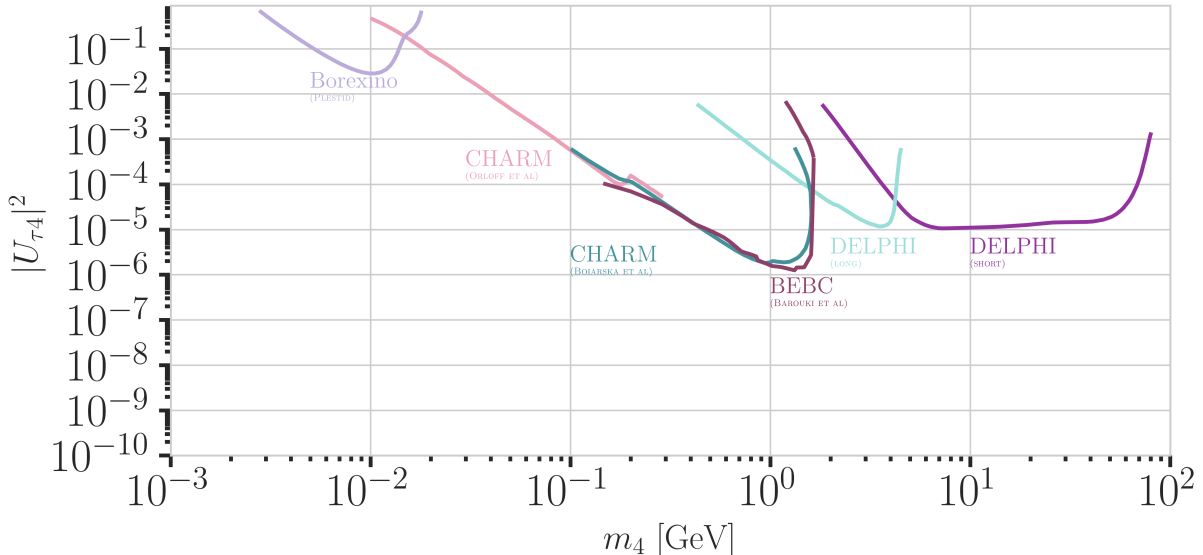


Figure 2.4: Current leading $|U_{\tau 4}|^2 - m_4$ upper limits from BOREXINO [62], CHARM [57, 58], DELPHI [43], and BEBC [44]. Modified from [51].

Nuclear Decays Measurements

A novel approach of searching for irregularities in energy-momentum conservation measurements in nuclear reactions might be a viable way of searching for HNLs, as they could be interpreted as constraints on $|U_{e4}|^2$ and m_4 .

Kinks in **beta decay** spectra would show up at $Q - m_4 c^2$, where the HNL mass, m_4 , can be measured between the lower energy detection threshold and the energy released in the decay, which is called Q value. Analyses using the tritium decay, with $Q = 18.6$ keV, are planned in *KATRIN* [63] and *TRISTAN* [64] in the 1 keV to 18 keV range. Their projected statistical limits are around 10^{-7} for $|U_{e4}|^2$, but will require further detector upgrades [64]. A first result from KATRIN measurements during commissioning sets limits at the order of 10^{-2} to 10^{-3} in the mass range of 0.1 keV to 1.6 keV [65]. *DUNE* is planning to measure the ionization charge of atmospheric argon decays, with $Q = 565$ keV, to probe $|U_{e4}|^2$ at in the 20 keV to 450 keV mass range. The projected sensitivity is at the 10^{-5} level, and might improve to 10^{-7} with additional detector improvements [66].

To test for the existence of HNLs using **electron capture** measurements, total energy-momentum reconstruction of all non-neutrino final states is needed. Electron capture is a pure two-body decay process, where the recoiling atom and the electron neutrino are the only final state particles, but additional energy is carried away by the de-excitation x-ray or auger electron. The energy-momentum conservation can be probed by measuring the atom and the associated de-excitation products. The mixing $|U_{e4}|^2$ can be probed by looking for a separated non-zero missing mass peak. The *BeEST* experiment has set limits at the 10^{-4} level in the 100 keV to 850 keV mass range, using berillium-7, which has a Q value of 862 keV. After planned upgrades to the experiment, the sensitivity is expected to improve to the 10^{-7} level [67].

Reactor searches up to 12 MeV in mass are possible at short baseline experiments using commercial or research reactors, which are a strong source

[61]: Aaij et al. (2021), "Search for heavy neutral leptons in $W^+ \rightarrow \mu^+ \mu^\pm$ jet decays"

mention the Z boson decay results from DELPHI (because they are strong in Utau4, too (RED))

[63]: Osipowicz et al. (2001), "KATRIN: A Next generation tritium beta decay experiment with sub-eV sensitivity for the electron neutrino mass. Letter of intent"

[64]: Mertens et al. (2019), "A novel detector system for KATRIN to search for keV-scale sterile neutrinos"

[65]: Aker et al. (2023), "Search for keV-scale sterile neutrinos with the first KATRIN data"

[66]: Abi et al. (2020), "Deep Underground Neutrino Experiment (DUNE), Far Detector Technical Design Report, Volume II: DUNE Physics"

[67]: Friedrich et al. (2021), "Limits on the Existence of sub-MeV Sterile Neutrinos from the Decay of ${}^7\text{Be}$ in Superconducting Quantum Sensors"

of electron antineutrinos and could therefore also produce HNLs if $|U_{e4}|^2$ is non-zero. Visible decay channels at these energies are $\nu_4 \rightarrow \nu_e e^+ e^-$, $\nu_4 \rightarrow \nu\gamma$, and $\nu_4 \rightarrow \nu\gamma\gamma$, where the first dominates. The first analysis in this field, reports limits at the 10^{-4} level in the 2 MeV to 7 MeV mass range [68].

[68]: Hagner et al. (1995), "Experimental search for the neutrino decay $\nu_3 + \nu_j + e^+ + e^-$ and limits on neutrino mixing"

Atmospheric and Solar Neutrinos

Natural sources of neutrinos are provided up to 20 MeV by the sun and up to 100s of GeV by neutrino production in the atmosphere. Both fluxes contain all flavors of neutrinos, due to mixing and oscillations, and can therefore be used to directly probe the mixings with ν_e , ν_μ , and ν_τ . Depending on the HNL mass and the strength of the mixing, which both govern the decay length, different signatures can be used to experimentally access large regions of the HNL parameter space. The strength of the mixing determines the total rate of HNL events, which is additionally affected by whether solely the minimal mass mixing is assumed, or also more complicated mixing scenarios, like the dipole portal, are considered.

So far, only very few analyses exist, which are performed by the experimental collaborations themselves. Several external theoretical groups have predicted the expected sensitivities to HNLs, produced from solar or atmospheric neutrinos, based on various coupling scenarios and decay lengths. A selection of the potential analyses will be discussed in the following.

For very long-lived particles, **production inside the sun** can be used as a source to search for HNLs in detectors on earth. This will only allow production through non-zero $|U_{e4}|^2$, because the initial solar neutrino flux is only ν_e . By searching for HNL decays to a SM neutrino and an electron positron pair $\nu_4 \rightarrow \nu_e e^+ e^-$ and comparing to the expected inter planetary positron flux, *Borexino* has placed the strongest limits on the mixing $|U_{e4}|^2$ at the order of 10^{-5} in the few MeV mass range [39].

For HNL decay length scales of the order of the Earth's diameter, **HNL up-scattering outside the detector** is possible, where a neutrino from the solar or the atmospheric neutrino flux scatters in the Earth and transfers some kinetic energy to the HNL, which can then later decay inside the detector. For HNL masses below 18 MeV produced from solar neutrinos, (external) limits were derived using the *Borexino* data for purely tau coupling through mass mixing [62] and for all flavor coupling through the dipole portal [69]. At similar decay length scales, the HNL could also be produced directly in the atmosphere, but neither this channel, nor the production anywhere in the Earth from atmospheric neutrinos has been investigated yet.

If the HNL decay lengths are sufficiently short, **production and decay in the detector** can happen and the observation of two vertices could be used to constrain the mixing parameters. In principle, this could be possible with any neutrino flavor produced in the sun or the atmosphere, but so far only theoretical studies have been performed for mass-mixing and dipole-portal couplings for the atmospheric neutrino detectors *IceCube* [70, 71] and *Super-K*, *Hyper-K*, and *Dune* [72, 73]. Due to the high complexity of these experiments, several simplified assumptions were made in the studies, which might not hold in reality, and the results should be taken with caution. For reliable sensitivity estimates and limits the collaborations should perform their own analyses.

[39]: Bellini et al. (2013), "New limits on heavy sterile neutrino mixing in B8 decay obtained with the *Borexino* detector"

[62]: Plestid (2021), "Luminous solar neutrinos I: Dipole portals"

[69]: Plestid (2021), "Luminous solar neutrinos II: Mass-mixing portals"

[70]: Coloma et al. (2017), "Double-Cascade Events from New Physics in *Icecube*"

[71]: Coloma (2019), "Icecube/Deep-Core tests for novel explanations of the *MiniBooNE* anomaly"

[72]: Atkinson et al. (2022), "Heavy Neutrino Searches through Double-Bang Events at Super-Kamiokande, DUNE, and Hyper-Kamiokande"

[73]: Coloma et al. (2021), "GeV-scale neutrinos: interactions with mesons and DUNE sensitivity"

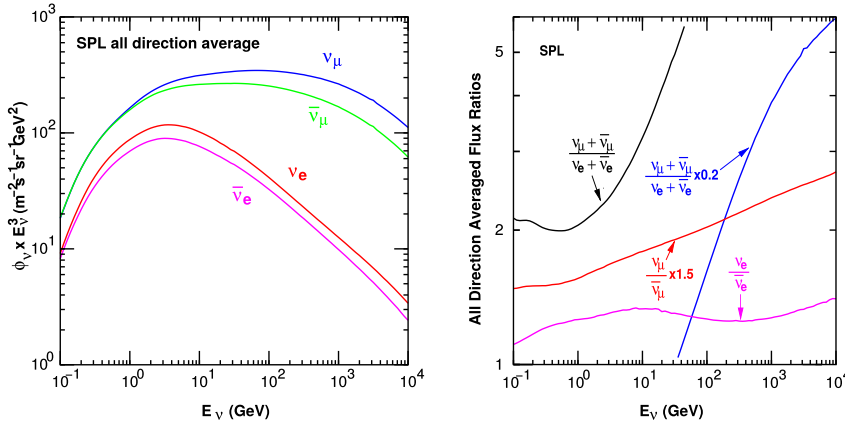


Figure 2.5: The atmospheric fluxes of different neutrino flavors as a function of energy (left) and the ratios between muon neutrinos and electron neutrinos as well as the ratios between neutrinos and antineutrinos for both those flavors (right). Results from the calculations performed for the geographic South Pole, taken from [75].

2.3 Atmospheric Neutrinos as Source of Heavy Neutral Leptons

This work focuses on the search for HNLs using atmospheric neutrinos as source for the production and decay inside the IceCube detector. The following sections will give a brief overview of the production of neutrinos in the atmosphere and the oscillations they undergo, before discussing the expected signatures of HNLs in the detector, where they are produced from the incoming neutrinos and subsequently decay.

2.3.1 Production of Neutrinos in the Atmosphere

The analysis performed in this work is based on the sample of neutrinos observed in IceCube DeepCore at energies below 100 GeV. At these energies, the flux exclusively originates in the Earth's atmosphere. Highly relativistic cosmic rays (protons and heavier nuclei [74]) interact in the upper atmosphere, producing showers of secondary particles. Neutrinos are produced in decays of charged pions and kaons (π and K mesons) present in those showers, where the dominant contribution comes from the decay chain

$$\begin{aligned} \pi^\pm &\rightarrow \mu^\pm + \nu_\mu(\bar{\nu}_\mu), \\ \mu^\pm &\rightarrow e^\pm + \bar{\nu}_\mu(\nu_\mu) + \nu_e(\bar{\nu}_e), \end{aligned} \quad (2.22)$$

where muon neutrinos ν_μ and muons μ^\pm are produced in the first decay and both electron and muon neutrinos $\nu_{e/\mu}$ are produced in the second decay. Atmospheric muons, which are also produced in these decays, are the main background component for IceCube DeepCore analyses.

The different atmospheric flux components are shown in Figure 2.5 (left), for a much broader energy range than relevant for this work. Both neutrinos and antineutrino fluxes are shown for electron and muon neutrinos and all fluxes are the directionally averaged expectation calculated at the South Pole. Muon neutrinos are dominating the flux and from Equation 2.22 the naive assumption would be that the ratio between muon and electron neutrinos is $(\nu_\mu + \bar{\nu}_\mu)/(\nu_e + \bar{\nu}_e) = 2$. This is roughly true at energies below 1 GeV, where all muons decay in flight, but at larger energies muons can reach the detector before decaying, which increases the ratio to approximately 10:1 at around 100 GeV. Additionally, kaon decays start to contribute which also increases the number of muons and muon neutrinos. The increasing ratio can be seen

[74]: Tanabashi et al. (2018), "Review of Particle Physics"

in Figure 2.5 (right), which also shows the ratio between neutrinos and antineutrinos for both flavors.

[76]: Fedynitch et al. (2015), “Calculation of conventional and prompt lepton fluxes at very high energy”

Say something about atmospheric neutrino flux uncertainties, based on recent JP/Anatoli papers. (YELLOW)

Charged mesons or tau particles can also be produced in cosmic ray interactions. Their decays lead to the production of tau neutrinos. At the energies relevant for this work however, the resulting tau neutrino flux is negligible as compared to the muon neutrino flux [76] and is not considered in the analysis. This is because both charged mesons and tau particles are much heavier than pions and kaons and therefore their production is suppressed at high energies.

2.3.2 Neutrino Oscillations

Describing neutrinos in their mass state as introduced in Section ?? is crucial to understand their propagation through space and time and to explain neutrino oscillations. Oscillations mean that a neutrino changes from its initial flavor, that it was produced with, to another flavor and back after traveling a certain distance.

The neutrino propagation in vacuum can be expressed by applying a plane wave approach, where the mass eigenstates evolve as

$$|\nu_k(t)\rangle = e^{-iE_k t/\hbar} |\nu_k\rangle . \quad (2.23)$$

The energy of the mass eigenstate $|\nu_k\rangle$ is $E_k = \sqrt{\vec{p}^2 c^2 + m_k^2 c^4}$, with momentum \vec{p} and mass m_k , \hbar is the reduced Planck constant, and c is the speed of light in vacuum. A neutrino is produced as a flavor eigenstate $|\nu_\alpha\rangle$ in a CC weak interaction, but its propagation happens as the individual mass states it is composed of. The probability of finding the neutrino with initial flavor $|\nu_\alpha\rangle$ in the flavor state $|\nu_\beta\rangle$ after the time t is calculated as

$$P_{\nu_\alpha \rightarrow \nu_\beta}(t) = |\langle \nu_\beta | \nu_\alpha(t) | \nu_\beta \rangle|^2 , \quad (2.24)$$

[77]: Dirac (1927), “The Quantum Theory of the Emission and Absorption of Radiation”

by applying Fermi’s Golden Rule [77], which defines the transition rate from one eigenstate to another by the strength of the coupling between them. This coupling strength is the square of the matrix element and using the fact that the mixing matrix is unitary ($U^{-1} = U^\dagger$) to describe the mass eigenstates as flavor eigenstates, we find the time evolution of the flavor state $|\nu_\alpha(t)\rangle$, which can be inserted into Equation 2.24 to find the probability as

$$P_{\nu_\alpha \rightarrow \nu_\beta}(t) = \sum_{j,k} U_{\beta j}^* U_{\alpha j} U_{\beta k} U_{\alpha k}^* e^{-i(E_k - E_j)t/\hbar} . \quad (2.25)$$

The indices j and k run over the mass eigenstates.

We can approximate the energy as

$$E_k \approx E + \frac{c^4 m_k^2}{2E} \longrightarrow E_k - E_j \approx \frac{c^4 \Delta m_{kj}^2}{2E} , \quad (2.26)$$

for small neutrino masses compared to their kinetic energy. Here, $\Delta m_{kj}^2 = m_k^2 - m_j^2$ is the mass-squared splitting between states k and j . Replacing the time in Equation 2.25 by the distance traveled by relativistic neutrinos

$t \approx L/c$ we get

$$\begin{aligned} P_{\nu_\alpha \rightarrow \nu_\beta}(t) &= \delta_{\alpha\beta} - 4 \sum_{j>k} \text{Re}(U_{\beta j}^* U_{\alpha j} U_{\beta k} U_{\alpha k}^*) \sin^2 \left(\frac{c^3 \Delta m_{kj}^2}{4E\hbar} L \right) \\ &\quad + 2 \sum_{j>k} \text{Im}(U_{\beta j}^* U_{\alpha j} U_{\beta k} U_{\alpha k}^*) \sin^2 \left(\frac{c^3 \Delta m_{kj}^2}{4E\hbar} L \right), \end{aligned} \quad (2.27)$$

which is called the survival probability if $\alpha = \beta$, and the transition probability if $\alpha \neq \beta$. Once again, this probability is only non-zero if there are neutrino mass eigenstates with masses greater than zero. Additionally, there must be a mass-squared difference Δm^2 and non-zero mixing between the states. Since we assumed propagation in vacuum in Equation 2.23, the transition and survival probabilities correspond to vacuum mixing.

[74]: Tanabashi et al. (2018), "Review of Particle Physics"

The mixing matrix can be parameterized as [74]

$$U = \begin{pmatrix} 1 & 0 & 0 \\ 0 & c_{23} & s_{23} \\ 0 & -s_{23} & c_{23} \end{pmatrix} \begin{pmatrix} c_{13} & 0 & s_{13} e^{-i\delta_{CP}} \\ 0 & 1 & 0 \\ -s_{13} e^{i\delta_{CP}} & 0 & c_{13} \end{pmatrix} \begin{pmatrix} c_{12} & s_{12} & 0 \\ -s_{12} & c_{12} & 0 \\ 0 & 0 & 1 \end{pmatrix}, \quad (2.28)$$

where $c_{ij} = \cos \theta_{ij}$ and $s_{ij} = \sin \theta_{ij}$ are cosine and sine of the mixing angle θ_{ij} , that defines the strength of the mixing between the mass eigenstates i and j , and δ_{CP} is the neutrino CP-violating phase. Experiments are sensitive to different mixing parameters, depending on the observed energy range, neutrino flavor, and the distance between the source and the detector L , commonly referred to as *baseline*. To be able to resolve oscillations the argument

$$\frac{\Delta m^2 L}{4E} \quad (2.29)$$

should be at the order of 1. This divides experiments into ones that are sensitive to very slow oscillations from $\Delta m_{21}^2 \approx \mathcal{O}(10^{-5} \text{eV}^2)$ and ones that are sensitive to faster oscillations from $\Delta m_{31}^2 \approx \mathcal{O}(10^{-3} \text{eV}^2)$. Relevant for this work are the parameters that can be measured at the earth's surface using atmospheric neutrinos, which are Δm_{31}^2 , θ_{23} , and θ_{13} , because the flux is primarily composed of muon neutrinos and antineutrinos. Applying the parameterization from Equation 2.28 to Equation 2.27 and using the fact that θ_{13} is small and θ_{12} is close to $\pi/4$, the survival probability of muon neutrinos can be approximated as

$$\begin{aligned} P_{\nu_\mu \rightarrow \nu_\mu} &\simeq 1 - 4|U_{\mu 3}|^2(1 - |U_{\mu 3}|^2) \sin^2 \left(\frac{\Delta m_{31}^2 L}{4E} \right) \\ &\simeq 1 - \sin^2(2\theta_{23}) \sin^2 \left(\frac{\Delta m_{31}^2 L}{4E} \right), \end{aligned} \quad (2.30)$$

while the tau neutrino appearance probability is

$$\begin{aligned} P_{\nu_\mu \rightarrow \nu_\tau} &\simeq 4|U_{\mu 3}|^2|U_{\tau 3}|^2 \sin^2 \left(\frac{\Delta m_{31}^2 L}{4E} \right) \\ &\simeq \sin^2(2\theta_{23}) \sin^2 \left(\frac{\Delta m_{31}^2 L}{4E} \right). \end{aligned} \quad (2.31)$$

The latest global fit [78] of all the parameters is shown in Table 2.2.

Parameter	Global Fit
θ_{12} [°]	$33.41^{+0.75}_{-0.72}$
θ_{13} [°]	$8.54^{+0.11}_{-0.10}$
θ_{23} [°]	$49.1^{+1.0}_{-1.3}$
Δm_{21}^2 [10^{-5}eV^2]	$7.41^{+0.21}_{-0.20}$
Δm_{31}^2 [10^{-3}eV^2]	$2.511^{+0.028}_{-0.027}$
δ_{CP} [°]	197^{+42}_{-25}

Table 2.2: Results from the latest global fit of neutrino mixing parameters from [78].

[78]: Esteban et al. (2020), "The fate of hints: updated global analysis of three-flavor neutrino oscillations"

say something about matter effect? (ORANGE)

say something about mass ordering? (ORANGE)

2.3.3 Neutrino Interactions with Nuclei

The neutrino detection principle of IceCube DeepCore is explained in Chapter ?? and relies on the weak interaction processes between neutrinos and the nuclei of the Antarctic glacial ice. At neutrino energies above 5 GeV, the cross-sections are dominated by *deep inelastic scattering (DIS)*, where the neutrino is energetic enough to resolve the underlying structure of the nucleons and interact with one of the composing quarks individually. As a result the nucleon breaks and a shower of hadronic secondary particles is produced. Depending on the type of interaction, the neutrino either remains in the final state for NC interactions or is converted into its charged lepton counterpart for CC interactions. The CC DIS interactions have the form

$$\begin{aligned} \nu_l + N &\rightarrow l^- + X , \\ \bar{\nu}_l + N &\rightarrow l^+ + X , \end{aligned} \quad (2.32)$$

where $\nu_l/\bar{\nu}_l$ and l^-/l^+ are the neutrino/antineutrino and its corresponding lepton/antilepton, and l can be either an electron, muon, or tau. N is the nucleon and X stands for any set of final state hadrons. The NC DIS interactions are

$$\begin{aligned} \nu_l + N &\rightarrow \nu_l + X \text{ and} \\ \bar{\nu}_l + N &\rightarrow \bar{\nu}_l + X . \end{aligned} \quad (2.33)$$

Figure 2.6 shows the Feynman diagrams for both processes DIS interactions

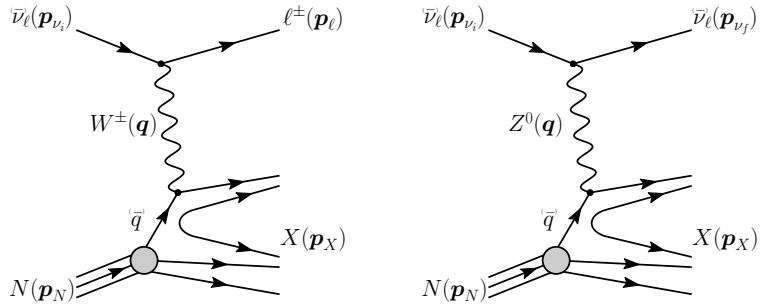


Figure 2.6: Feynman diagrams for deep inelastic scattering of a neutrino with a nucleon via charged-current (left) and neutral current (right) interactions. ν_{ν_i} , p_{ν_i} and p_{ν_f} , p_l , p_N are the input and output four-momenta, while q is the momentum transfer. Taken from [79].

have a roughly linear energy dependent cross-section above ~ 20 GeV and are well measured and easy to theoretically calculate. They are the primary interaction channel for neutrinos detected with IceCube.

At energies below 5 GeV, *quasi-elastic scattering (QE)* and *resonant scattering (RES)* become important. At these energies the neutrinos interact with the approximately point-like nucleons, without breaking them up in the process. RES describes the process of a neutrino scattering off a nucleon producing an excited state of the nucleon in addition to a charged lepton. It is the dominant process at 1.5 GeV to 5 GeV for neutrinos and 1.5 GeV to 8 GeV for antineutrinos. Below 1.5 GeV QE is the main process, where protons are converted to neutrons in antineutrino interactions and vice-versa for neutrino interactions. Additionally, a charged lepton corresponding to the neutrino/antineutrino flavor is produced. The cross-sections of QE and RES scattering processes are not linear in energy and the transition region from QE/RES to DIS is poorly understood. The total cross-sections and their composition is shown in Figure 2.7. It can be seen that the interaction cross-sections are very small at the order of 10^{-38} cm 2 . This is the reason why very

large volume detectors are required to measure atmospheric neutrinos with sufficient statistics to perform precision measurements of their properties. The interaction length of a neutrino with $E_\nu = 10 \text{ GeV}$ is of $\mathcal{O}(10 \times 10^{10} \text{ km})$, for example.

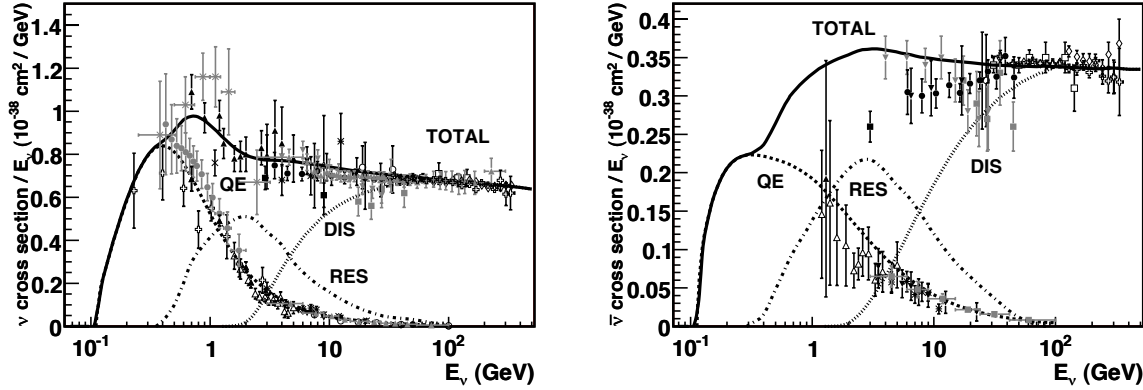


Figure 2.7: Total neutrino (left) and antineutrino (right) per nucleon cross-section divided by neutrino energy plotted against energy. The three main scattering processes quasi-elastic scattering (QE), resonant scattering (RES), and deep-inelastic scattering (DIS) are shown. Taken from [80].

2.3.4 Heavy Neutral Lepton Production and Decay

For the search conducted in this work, both production and decay are assumed to happen inside the detector, therefore probing decay lengths ranges at the scale of the detector size, which is below 1000 m. Since the mixing with the first two generations of leptons is already strongly constrained as was discussed in Section 2.3, only the mixing with the tau neutrino will be considered in the following. Due to the effect of oscillations, described in Section 2.3.2, the initial atmospheric muon neutrino flux provides a sizable tau neutrino flux at the detector.

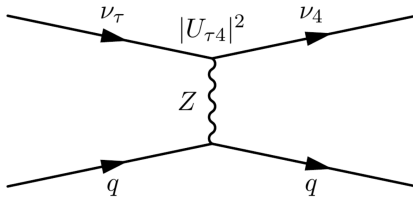


Figure 2.8: Feynman diagram of the HNL production. The heavy mass state is produced in the up-scattering of a tau neutrino.

For a non-zero $|U_{\tau 4}|^2$, the HNL can be produced through **up-scattering in the ice**. An incoming tau neutrino scatters on an ice nucleus and transfers some of its kinetic energy to the heavy neutrino. The Feynman diagram of this process is shown in Figure 2.8. The custom NC cross-sections calculated for this purpose are explained in more detail in Section 3.2.1, but are similar to the SM tau neutrino NC cross-sections, with a reduction scaling with the mixing $|U_{\tau 4}|^2$ and energy dependent reductions, due to kinematic constraints because of the heavy neutrino mass. The scattering process produces a hadronic cascade, which will produce light in the detector.

After a certain distance, the HNL will **decay in the ice**, where the possible decay channels considered in this work are shown in Figure 2.9 and the underlying, explicit calculations are discussed in Section 3.2.1. The decay can be a CC or NC and both purely leptonic and leptonic+mesonic modes

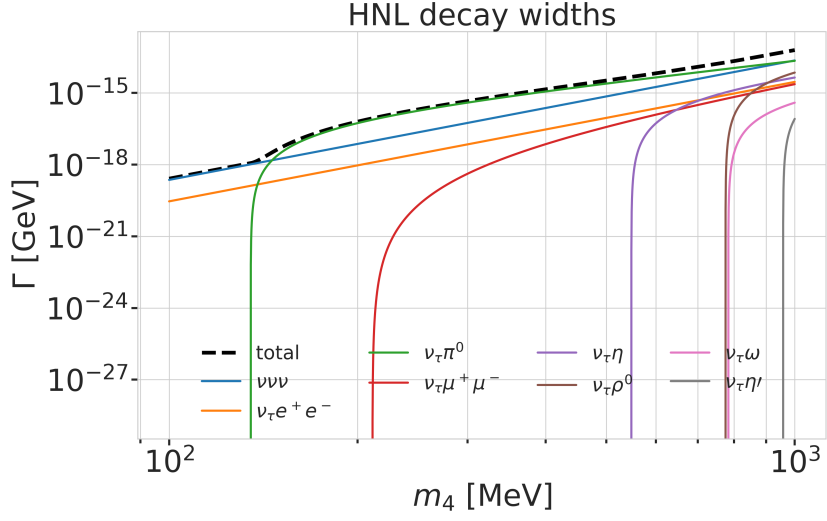
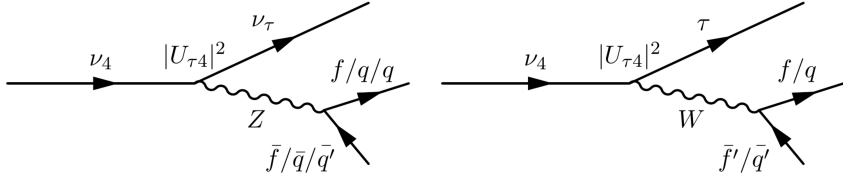


Figure 2.9: Decay widths of the HNL within the mass range considered, calculated based on the results from [73]. Given the existing constraints on $|U_{e4}|^2$ and $|U_{\mu 4}|^2$, we consider that the corresponding decay modes are negligible.

Figure 2.10: Feynman diagram of the HNL decay. The heavy mass state can decay through neutral current interaction (left) into a tau neutrino and a charged lepton or quark pair, or through charged current interaction (right) into a tau lepton and a charged lepton or quark.



are possible. The Feynman diagrams of the decays can be seen in Section ???. Only the mass range relevant for this work is presented and mixing with $\nu_{e/\mu}$ is assumed to be negligible. Depending on the decay channel, an electromagnetic or a hadronic cascade is produced, while some energy is carried away by the invisible neutrino. The decay length of the HNL is defined by its proper lifetime¹, which is given by

$$\tau_{\text{proper}} = \frac{\hbar}{\Gamma_{\text{total}}(m_4) \cdot |U_{\tau 4}|^2}, \quad (2.34)$$

where \hbar is the reduced Planck constant, $\Gamma_{\text{total}}(m_4)$ is the total decay width of the HNL for the given mass, and $|U_{\tau 4}|^2$ is the mixing with the tau neutrino. The total decay width is the sum of the partial decay widths for all possible decay channels. The mean lab frame decay length is then given by

$$L_{\text{decay}} = \gamma v \tau_{\text{proper}}, \quad (2.35)$$

where γ is the Lorentz factor of the HNL, defined by the kinetic energy. This will be further discussed on Section 3.2.1. Figure 2.11 shows the mean decay lengths for an example mass of $m_4 = 0.6$ GeV and several mixing values.

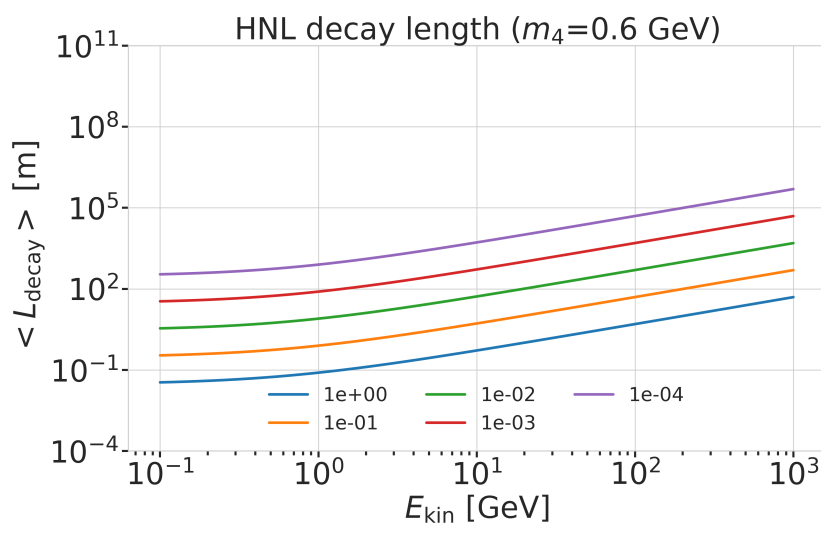


Figure 2.11: Theoretical mean decay length of the HNL for a mass of 0.6 GeV and different mixing values.

The central part of this thesis is the HNL signal simulation itself. Since this is the first search for HNLs with IceCube DeepCore, there was no prior knowledge of the number of events expected per year nor of the expected performance in terms of reconstruction and classification accuracy. This chapter describes the first HNL event generation developed for IceCube DeepCore. Two avenues of generation were pursued in parallel. A collection of model-independent simulation samples is explained in Section 3.1. They were used for performance benchmarking and for cross-checks to validate the physically accurate, model-dependent simulation, which is described in Section 3.2. For completeness, the event generation for SM background events is briefly described in Section 3.3. The default low-energy event selection and processing chain, which is applied identically to both background and signal, is introduced in Chapter ??.

3.1	Model-Independent Simulation	23
3.2	Model-Dependent Simulation	26
3.3	Background Simulation	32

JVS: I would describe simulation sets you produced in past rather than present tense (ORANGE)

3.1 Model-Independent Simulation

To investigate the potential of IceCube to detect HNLs by identifying the unique double cascade morphology explained in Section 2.3.4, a model-independent double cascade generator was developed, where the kinematics of each cascade can be controlled directly. Using this generator, several simulation samples were produced to investigate the performance of IceCube DeepCore to detect low-energy double cascades, dependent on their properties. All samples are produced using a collection of custom generator functions [81] that place two EM cascade vertices with variable energy and direction at configurable locations in the detector.

3.1.1 Simplistic Samples

To investigate the best-case and the worst-case double cascade event scenarios, two samples are produced in the DeepCore volume: straight up-going events ($\cos(\theta) = -1$) that are centered on a string and horizontal events ($\cos(\theta) = 0$). The first sample is used to investigate one of the most promising scenarios to detect a double cascade, where both cascade centers are located on a DeepCore string and the directions are directly up-going. One of the DeepCore strings was randomly chosen as the x - y coordinate for this sample. As already mentioned in Section ??, DeepCore strings have higher quantum efficiency DOMs and a denser vertical spacing, making them better to detect low-energy events that produce little light. To produce the events, the x, y position of the cascades is fixed to the center of the string while the z positions are each sampled uniformly along the axis of the string. Note that this will therefore not produce a uniform length distribution between the cascades. The positions are defined in the IceCube coordinate system that was introduced in Section ??.

The energies are sampled uniformly between 0.0 GeV and 60.0 GeV, to generously cover the region where $\nu_\mu \rightarrow \nu_\tau$ appearance is maximized. The time of the lower cascade is set to $t_0 = 0.0$ ns and for the upper one to $t_1 = L/c$, assuming the HNL travels at the speed of

add/move event views to here? or draw a schematic of these events? (ORANGE)

light, c . Figure 3.1 shows the resulting energy distributions and the decay length distribution, where it can be seen how the uniform cascade energies sum into a non-uniform total energy, and the decay length distribution is also non-uniform due to the uniform z sampling of both cascades, which sets the distance between them.

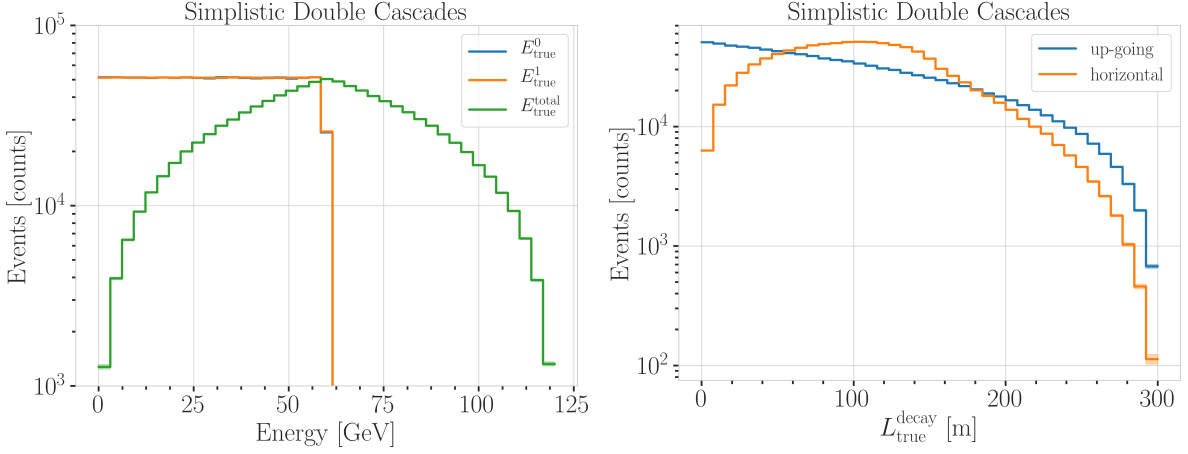


Figure 3.1: Generation level distributions of the simplistic simulation samples. Cascade and total energies (left) and decay lengths (right) of both samples are shown.

The second sample is used to investigate the reconstruction performance for horizontal events, where the spacing between DOMs is much larger. The cascades are placed uniformly on a circle with radius of $r = 150$ m centered in DeepCore at the depth of $z = -330$ m. The direction is always horizontal and azimuth is defined by the connecting vector of both cascade positions. The energies are again sampled uniformly between 0.0 GeV and 60.0 GeV. The specific sampling distributions/values for the cascades are listed in Table 3.1, for both samples and for completeness, all distributions are shown in Figure A.2.

Table 3.1: Generation level sampling distributions and ranges/values of up-going and horizontal model-independent simulation.

Sample	Variable	Distribution	Range/Value
Up-going			
	energy	uniform	0.0 GeV to 60.0 GeV
	zenith	fixed	180.0°
	azimuth	fixed	0.0°
	x, y position	fixed	(41.6, 35.49) m
	z position	uniform	-480.0 m to -180.0 m
Horizontal			
	energy	uniform	0.0 GeV to 60.0 GeV
	zenith	fixed	90.0°
	azimuth	uniform	0.0° to 360.0°
	x, y position	uniform (circle)	$c=(46.29, -34.88)$ m, $r=150.0$ m
	z position	fixed	-330.0 m

3.1.2 Realistic Sample

To thoroughly investigate the potential of IceCube DeepCore to detect double cascade events, a more realistic simulation sample is produced that aims to be as close as possible to the expected signal simulation explained in Section 3.2, while still allowing additional freedom to control the double cascade kinematics. This sample is particularly useful for validating the model-dependent HNL simulation described in Section 3.2.

For this purpose the total energy is sampled from an E^{-2} power law, mimicking the energy spectrum of the primary neutrinos as stated in Section 3.3.1. The total energy is divided into two parts, by assigning a fraction between 0 % and 100 % to one cascade and the remaining part to the other cascade. This is a generic approximation of the realistic process described in Section 3.2, and chosen such that the whole sample covers various cases of energy distributions between the two cascades. The decay length is sampled from an exponential distribution, as expected for a decaying heavy mass state. The resulting energy distributions and the decay length distribution are shown in Figure 3.2, where it can be seen that the individual cascade energies can be very small, due to splitting the total energy, and the decay lengths spans across several orders of magnitude.

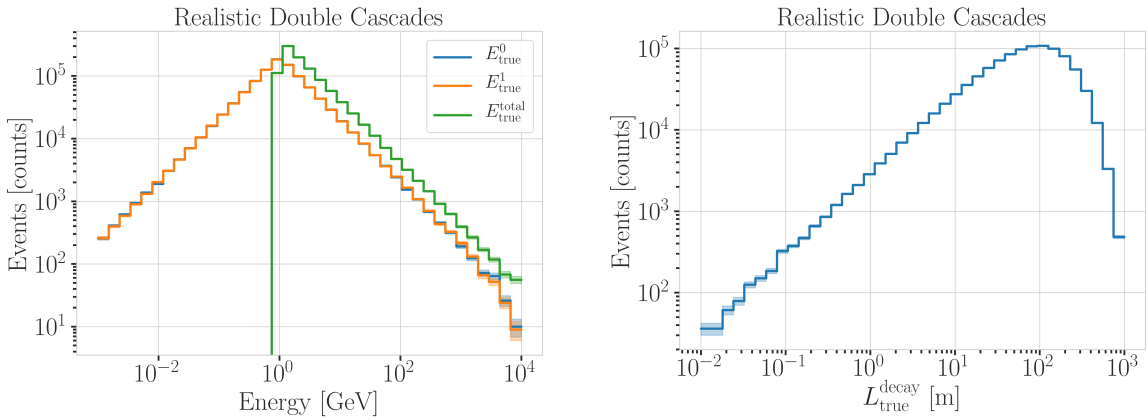


Figure 3.2: Generation level distributions of the realistic sample. Shown are the individual cascade energies and total energy (left) and decay lengths (right). It can be seen how the cascade energies can get very small, and the decay length follows a more realistic distribution spanning across several orders of magnitude.

To efficiently generate events in a way that produces distributions similar to what would be observed with DeepCore, one of the cascade positions is sampled inside the DeepCore volume by choosing its coordinates uniformly on a cylinder that is centered in DeepCore. This is similar to a trigger condition of one cascade always being inside the DeepCore fiducial volume. Choosing the direction of the event by sampling zenith and azimuth uniformly between 70° and 180° and 0° and 360°, respectively, the position of the other cascade can be inferred for a given decay length, assuming a travel speed of c , and choosing whether the cascade position that was sampled is the first cascade or the second with a 50 % chance. The zenith angle is chosen between straight up-going (zenith of 180°) and slightly down-going from above the horizon (70°) to mimic an event selection that reduces atmospheric muons by rejecting events coming from above the horizon, but still incorporates some down-going events. All distributions are shown in Figure A.2, and the sampling distributions/values are listed in Table 3.2.

Variable	Distribution	Range/Value
energy (total)	power law E^{-2}	1 GeV to 1000 GeV
decay length	exponential $e^{-0.01L}$	0 m to 1000 m
zenith	uniform	70° to 180°
azimuth	uniform	0° to 360°
x, y (one cascade)	uniform (circle)	$c=(46.29, -34.88)$ m, $r=150$ m
z (one cascade)	uniform	-480.0 m to -180.0 m

Table 3.2: Generation level sampling distributions and ranges/values of the realistic model-independent simulation.

3.2 Model-Dependent Simulation

[82]: Abbasi et al. (2021), “LeptonInjector and LeptonWeighter: A neutrino event generator and weighter for neutrino observatories”

[83]: Agostinelli et al. (2003), “Geant4—a simulation toolkit”
[84]: Rädel et al. (2012), “Calculation of the Cherenkov light yield from low energetic secondary particles accompanying high-energy muons in ice and water with Geant4 simulations”

To estimate the HNL event expectation in IceCube DeepCore, depending on the specific model parameters, a generator was developed that is based on the HNL theory introduced in Section 2.3. For this work, only the interaction with the τ -sector was taken into account ($|U_{\alpha 4}^2| = 0$, $\alpha = e, \mu$), which reduces the physics parameters of interest and relevant for the simulation to the fourth heavy lepton mass, m_4 , and the mixing, $|U_{\tau 4}^2|$. The generator uses a customized *LEPTONINJECTOR* (*LI*) version to create the events and *LEPTONWEIGHTER* (*LW*) to weight them [82]. The modified *LI* and the essential components needed for the HNL simulation are described in the next sections, followed by the description of the weighting scheme and the sampling distributions chosen for the generation.

3.2.1 Custom LeptonInjector

In its standard version, the *LI* generator produces neutrino interactions by injecting a lepton and a hadronic cascade at the interaction vertex of the neutrino, where the lepton is the charged (neutral) particle produced in a CC (NC) interaction and the cascade is the hadronic cascade from the breaking nucleus. The hadronic cascade is stored as a specific object of type *Hadrons*, which triggers the correct simulation of the shower development in the following simulation steps, identical to what is described for neutrinos in Section 3.3.1. Below 30 GeV the individual hadrons are simulated using *GEANT4* [83] while for higher energies an analytical approximation from [84] is used. The main differences to an EM cascade is that part of the energy will not be observed, because it goes into neutral particles, and that the spatial development of the shower is different as discussed in Section ???. Both objects are injected with the same (x, y, z, t) coordinates and the kinematics are sampled from the differential and total cross-sections that are one of the inputs to *LI*.

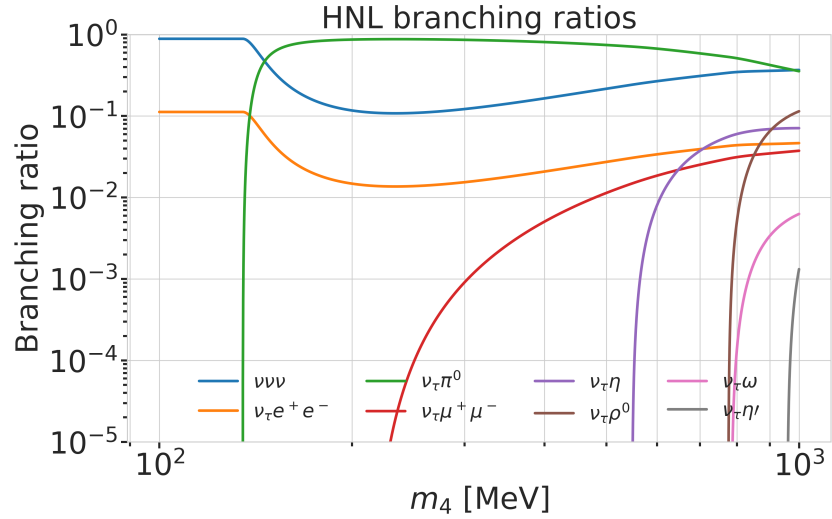


Figure 3.3: Branching ratios of the HNL within the mass range considered in this work, only considering $|U_{\tau 4}^2| \neq 0$, calculated based on the results from [73].

¹: The explicit sampling distributions and ranges can be found in Section 3.2.2.

In the modified version, the SM lepton at the interaction vertex is replaced by the new HNL particle, where the interaction cross-sections are replaced by custom, mass dependent HNL cross-sections. The HNL is forced to decay after a chosen distance¹ to produce secondary SM particles, where the decay

mode is chosen with a probability given by the mass dependent branching ratios from the kinematically accessible decay modes shown in Figure 3.3. The cross-section and decay width calculations were implemented for this purpose and will be explained in more detail in the following. Another addition to LI is that the decay products of the HNL are also stored. These HNL daughter particles form the second cascade, not as a single hadronic cascade object, but as the explicit particles forming the shower. They are injected with the correctly displaced position and delayed time from the interaction vertex, given the HNL decay length. The kinematics of the two-body decays are computed analytically, while the 3-body decay kinematics are calculated with `MADGRAPH` [85], which will also be explained further below. Independent of the number of particles in the final state of the HNL decay, the kinematics are calculated/simulated at rest and then boosted along the HNL momentum.

[85]: Alwall et al. (2014), “The automated computation of tree-level and next-to-leading order differential cross sections, and their matching to parton shower simulations”

The injection is done using the LI *volume mode*, for the uniform injection of the primary particle on a cylindrical volume, adding 50 % of the events with ν_τ and the other half with $\bar{\nu}_\tau$ as primary particle types. The generator takes the custom double-differential/total cross-section splines described below and the parameters defining the sampling distributions as inputs.

Cross-Sections

The cross-sections are calculated using the `NuXSSplMkr` [86] software, which is a tool to calculate neutrino cross-sections from *parton distribution functions (PDFs)* and then fit to an N-dimensional tensor-product B-spline surface [87] to produce the splines that can be read and used with LI/LW. The tool was modified to produce the custom HNL cross-sections, where the main modification to calculate the cross-sections for the ν_τ -NC interaction into the new heavy mass state, is the addition of a kinematic condition to ensure that there is sufficient energy to produce the heavy mass state. It is the same condition fulfilled for the CC case, where the outgoing charged lepton mass is non-zero. Following [88] (equation 7), the condition

$$(1 + x\delta_N)h^2 - (x + \delta_4)h + x\delta_4 \leq 0 \quad (3.1)$$

[87]: Whitehorn et al. (2013), “Penalized splines for smooth representation of high-dimensional Monte Carlo datasets”

[88]: Levy (2009), “Cross-section and polarization of neutrino-produced tau’s made simple”

is implemented for the NC case in the `NuXSSplMkr` code. Here

$$\delta_4 = \frac{m_4^2}{s - M^2}, \quad (3.2)$$

$$\delta_N = \frac{M^2}{s - M^2}, \text{ and} \quad (3.3)$$

$$h \stackrel{\text{def}}{=} xy + \delta_4, \quad (3.4)$$

with x and y being the Bjorken variables, m_4 and M the mass of the heavy state and the target nucleon, respectively, and s the center of mass energy squared. The custom version was made part of the open source `NuXSSplMkr` software and can thus be found in [86]. The result of this kinematic condition is that events cannot be produced for energy, x, y combinations that do not have sufficient energy to produce the outgoing, massive lepton. This results in a reduction of the cross-section towards lower energies, which scales with the assumed mass of the HNL. This effect can be seen in Figure 3.4.

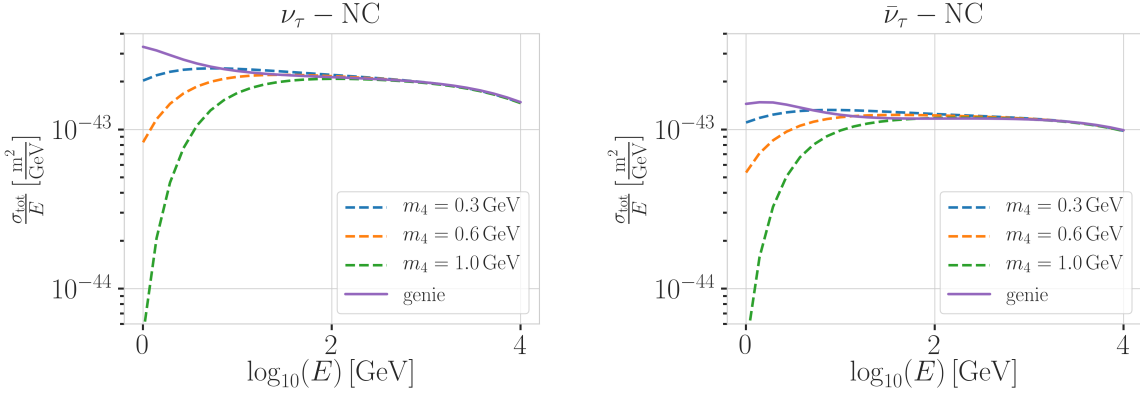


Figure 3.4: Custom HNL total cross-sections for the three target masses compared to the total ($\nu_\tau/\bar{\nu}_\tau$ NC) cross-sections used for SM neutrino simulation production with GENIE.

The GRV98LO PDFs were added to the cross-section spline maker and used to create the HNL cross-sections for consistency with the neutrino simulation explained in Section 3.3.1. The double-differential ($d^2\sigma/dxdy$) and total (σ) cross-sections were produced for the chosen target HNL masses and then splined in energy, x , and y for $d^2\sigma/dxdy$ and σ in the energy. Figure 3.4 shows the total cross-sections that were produced compared to the cross-section used for the production of the SM $\nu_\tau/\bar{\nu}_\tau$ NC background simulation. They agree above ~ 200 GeV, where the modification should not have any effect on the cross-sections. This is the desired result of using the identical input PDFs, and confirms that the unmodified cross-sections produced with NuXSSplMkr agree with the GENIE cross-sections.

Decay Channels

[73]: Coloma et al. (2021), “GeV-scale neutrinos: interactions with mesons and DUNE sensitivity”

Channel	Opens
$\nu_4 \rightarrow \nu_\tau \nu_\alpha \bar{\nu}_\alpha$	0 MeV
$\nu_4 \rightarrow \nu_\tau e^+ e^-$	1 MeV
$\nu_4 \rightarrow \nu_\tau \pi^0$	135 MeV
$\nu_4 \rightarrow \nu_\tau \mu^+ \mu^-$	211 MeV
$\nu_4 \rightarrow \nu_\tau \eta$	548 MeV
$\nu_4 \rightarrow \nu_\tau \rho^0$	770 MeV
$\nu_4 \rightarrow \nu_\tau \omega$	783 MeV
$\nu_4 \rightarrow \nu_\tau \eta'$	958 MeV

Table 3.3: Possible decay channels of the HNL, considering only $|U_{\tau 4}|^2 \neq 0$, and the mass at which each channel opens.

The accessible decay channels are dependent on the mass of the HNL and the allowed mixing. For this analysis, where only $|U_{\tau 4}|^2 \neq 0$, the decay channels considered are listed in Table 3.3 and the corresponding branching ratios are shown in Figure 3.3. The individual branching ratio for a specific mass is calculated as $\text{BR}_i(m_4) = \Gamma_i(m_4)/\Gamma_{\text{total}}(m_4)$, where $\Gamma_{\text{total}}(m_4) = \sum \Gamma_i(m_4)$. The individual decay widths Γ_i are computed using the state-of-the-art calculations from [73], which are described in the following.

2-Body Decay Widths The decay to a neutral pseudoscalar meson is

$$\Gamma_{\nu_4 \rightarrow \nu_\tau P} = |U_{\tau 4}|^2 \frac{G_F^2 m_4^3}{32\pi} f_P^2 (1 - x_p^2)^2, \quad (3.5)$$

with $x_p = m_p/m_4$ and the *effective decay constants* f_P given by

$$f_{\pi^0} = +0.1300 \text{ GeV}, \quad (3.6)$$

$$f_\eta = +0.0816 \text{ GeV}, \text{ and} \quad (3.7)$$

$$f_{\eta'} = -0.0946 \text{ GeV}, \quad (3.8)$$

while the decay to a neutral vector meson is given by

$$\Gamma_{\nu_4 \rightarrow \nu_\tau V} = |U_{\tau 4}|^2 \frac{G_F^2 m_4^3}{32\pi} \left(\frac{f_V}{m_V} \right)^2 g_V^2 (1 + 2x_V^2)(1 - x_V^2)^2 , \quad (3.9)$$

with $x_V = m_V/m_4$,

$$f_{\rho^0} = 0.171 \text{ GeV}^2 , \quad (3.10)$$

$$f_\omega = 0.155 \text{ GeV}^2 , \quad (3.11)$$

and

$$g_{\rho^0} = 1 - 2 \sin^2 \theta_w , \quad (3.12)$$

$$g_\omega = \frac{-2 \sin^2 \theta_w}{3} , \quad (3.13)$$

and $\sin^2 \theta_w = 0.2229$ [89], where θ_w is the Weinberg angle.

[89]: Tiesinga et al. (2021), “CODATA recommended values of the fundamental physical constants: 2018”

3-Body Decay Widths The (invisible) decay to three neutrinos, one of flavor τ and two of any flavor α , is

$$\Gamma_{\nu_4 \rightarrow \nu_\tau \nu_\alpha \bar{\nu}_\alpha} = |U_{\tau 4}|^2 \frac{G_F^2 m_4^5}{192\pi^3} , \quad (3.14)$$

while the decay to two charged leptons (using $x_\alpha = (m_\alpha/m_4)^2$) of the same flavor reads

$$\Gamma_{\nu_4 \rightarrow \nu_\tau l_\alpha^+ l_\alpha^-} = |U_{\tau 4}|^2 \frac{G_F^2 m_4^5}{192\pi^3} [C_1 f_1(x_\alpha) + C_2 f_2(x_\alpha)] , \quad (3.15)$$

with the constants defined as

$$C_1 = \frac{1}{4}(1 - 4 \sin^2 \theta_w + 8 \sin^4 \theta_w) , \quad (3.16)$$

$$C_2 = \frac{1}{2}(-\sin^2 \theta_w + 2 \sin^4 \theta_w) , \quad (3.17)$$

the functions as

$$f_1(x_\alpha) = (1 - 14x_\alpha - 2x_\alpha^2 - 12x_\alpha^3)\sqrt{1 - 4x_\alpha} + 12x_\alpha^2(x_\alpha^2 - 1)L(x_\alpha) , \quad (3.18)$$

$$f_2(x_\alpha) = 4[x_\alpha(2 + 10x_\alpha - 12x_\alpha^2)\sqrt{1 - 4x_\alpha} + 6x_\alpha^2(1 - 2x_\alpha + 2x_\alpha^2)L(x_\alpha)] , \quad (3.19)$$

and

$$L(x) = \ln \left(\frac{1 - 3x - (1 - x)\sqrt{1 - 4x}}{x(1 + \sqrt{1 - 4x})} \right) . \quad (3.20)$$

Analytical 2-Body Decay Kinematics

Following the review of [21], the 4-vector defining the kinematics of a particle is $p = (E, \vec{p})$, with its energy, E , and 3-momentum, \vec{p} . Squaring it gives the mass, $p^2 = E^2 - \vec{p}^2 = m^2$, while the velocity is $\vec{\beta} = \vec{p}/E$. If the HNL with mass m_4 decays into two particles with masses m_1 and m_2 , their 3-momenta

[21]: Workman et al. (2022), “Review of Particle Physics”

in the rest frame of the HNL are given by

$$|\vec{p}_1| = |\vec{p}_2| = \frac{\lambda^{1/2}(m_4^2, m_1^2, m_2^2)}{2m_4}, \quad (3.21)$$

where $\lambda(x, y, z) = x^2 + y^2 + z^2 - 2xy - 2xz - 2yz$. The energy of the particles is then given by

$$E_1 = \frac{m_4^2 + m_1^2 - m_2^2}{2m_4}, \quad (3.22)$$

and equivalently for E_2 . The 4-vectors of the particle are then boosted to the lab frame, where the HNL is moving with velocity $\vec{\beta}$.

Simulated 3-Body Decay Kinematics

The 3-body decay kinematics cannot be computed analytically, instead, we employ **MADGRAPH4** (v3.4.0) [90] for this purpose. MadGraph is a tool to simulate particle collisions and decay processes, and is widely used in the high-energy physics community. The 3-body decay kinematics are calculated in the rest frame of the HNL, using decay diagrams calculated with **FEYNRULES** 2.0 [91] and the Lagrangians derived in [73] as input. The *Universal FeynRules Output (UFO)* from **EFFECTIVE_HEAVYN_MAJORANA_v103** were used for our calculation. For each mass and corresponding decay channels, we produce 1×10^6 decay kinematic variations in the rest frame and store those in a text file. During event generation, we uniformly select an event from that list, to simulate the decay kinematics of a 3-body decay.

3.2.2 Sampling Distributions

Table 3.4: Generation level sampling distributions and ranges/values of the model-dependent simulation samples.

Variable	Distribution	Range/Value
energy	E^{-2}	[2 GeV, 1×10^4 GeV]
zenith	uniform (in $\cos(\theta)$)	[80°, 180°]
azimuth	uniform	[0°, 360°]
vertex x, y	uniform	$r=600$ m
vertex z	uniform	-600 m to 0 m
m_4	fixed	[0.3, 0.6, 1.0] GeV
L_{decay}	L^{-1}	[0.0004, 1000] m

In principle, the generation level sampling distributions should be chosen such that at the final level of the event selection chain the phase space relevant for the analysis is covered with sufficient statistics to make a reasonable estimate of the event expectation. Initial distributions insufficiently covering the phase space leads to an underestimation of the expected rates, because some of the events that would pass the selection are not produced. This limits the expected analysis potential. Three discrete simulation samples were produced with HNL masses of 0.3 GeV, 0.6 GeV, and 1.0 GeV. During development of the analysis it became clear that short decay lengths were undersampled at the final selection level. Therefore, each discrete mass sample consists of a part that is generated for very short decay lengths and one for long decay lengths. The remaining sampling distributions are identical for all samples and are listed in Table 3.4. The target number of

events for each sample was 2.5×10^9 at generation to result in sufficient MC statistics at final level. Figure 3.5 shows some selected generation level distributions. Additional distributions can be found in Figure A.3.

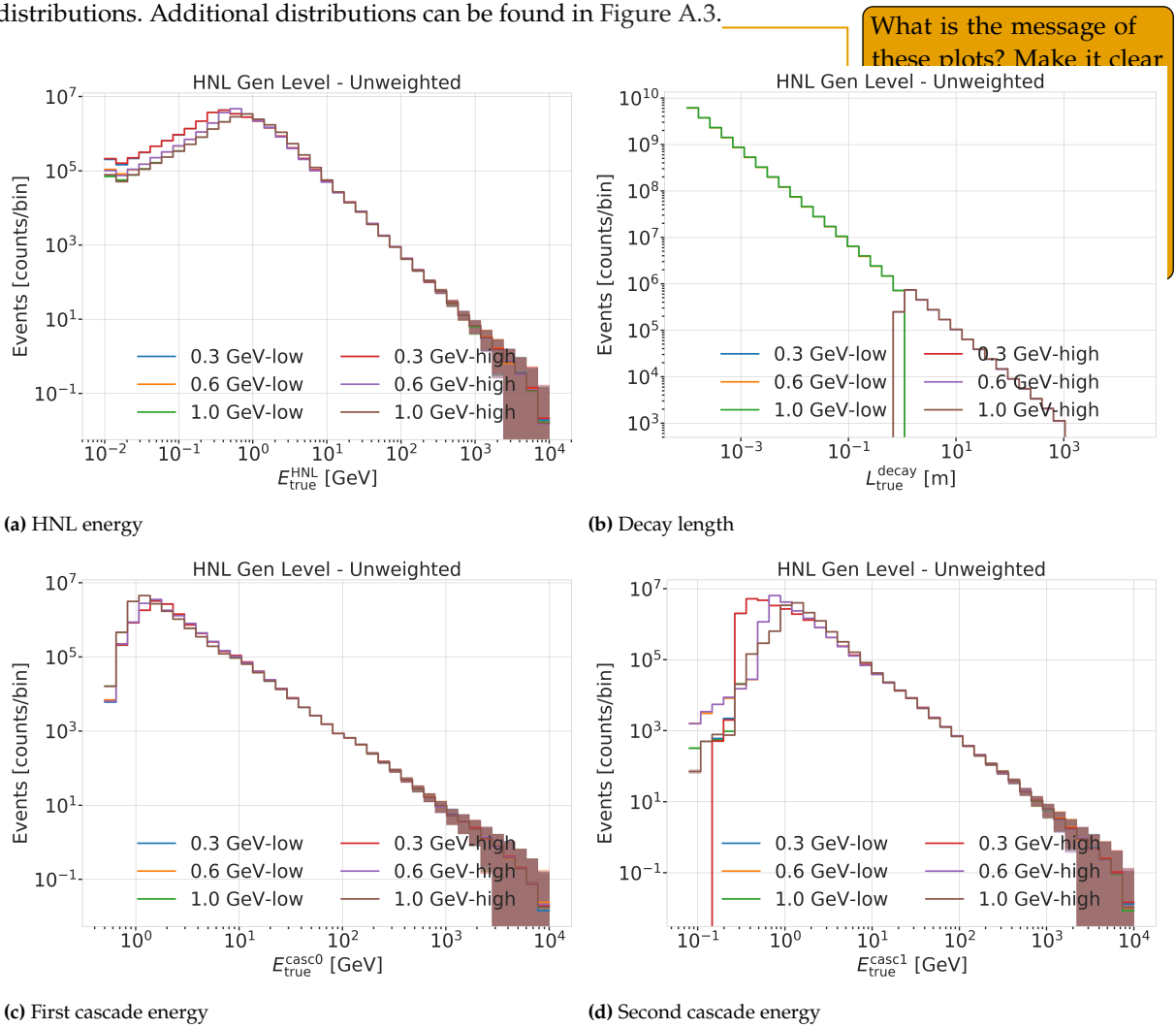


Figure 3.5: Generation level distributions of the model-dependent simulation.

3.2.3 Weighting Scheme

To produce physically correct event distributions based on the simplified generation sampling distributions for the HNL simulation, the forward folding method that was already introduced for the SM simulation in Section 3.3 is also used. The only required input is the mixing strength $|U_{\tau 4}|^2$, which is the variable physics parameter in this analysis. For each event the gamma factor

$$\gamma = \frac{\sqrt{E_{\text{kin}}^2 + m_4^2}}{m_4}, \quad (3.23)$$

is calculated, with the HNL mass m_4 , and its kinetic energy E_{kin} . The speed of the HNL is calculated as

$$v = c \cdot \sqrt{1 - \frac{1}{\gamma^2}}, \quad (3.24)$$

JVS: The build-up of the weight expression is hard to follow without knowing where it's going. It may be better to start with the fact that the importance sampling weight is the ratio of PDFs, then write down each pdf, then drill down into each of the terms (basically, the standard "tell me what you're going to tell me, then tell me, then tell me what you told me" scheme). (RED)

where c is the speed of light. With these, the lab frame decay length range $[s_{\min}, s_{\max}]$ can be converted into the rest frame lifetime range $[\tau_{\min}, \tau_{\max}]$ for each event

$$\tau_{\min/\max} = \frac{s_{\min/\max}}{v \cdot \gamma}. \quad (3.25)$$

The proper lifetime of each HNL event can be calculated using the total decay width Γ_{total} from Section ?? and the chosen mixing strength $|U_{\tau 4}|^2$ as

$$\tau_{\text{proper}} = \frac{\hbar}{\Gamma_{\text{total}}(m_4) \cdot |U_{\tau 4}|^2}, \quad (3.26)$$

where \hbar is the reduced Planck constant. Since the decay lengths or lifetimes of the events are sampled from an inverse distribution instead of an exponential, as it would be expected from a particle decay, we have to re-weight accordingly to achieve the correct decay lengths or lifetimes distribution. This is done by using the wanted exponential distribution

$$\text{PDF}_{\text{exp}} = \frac{1}{\tau_{\text{proper}}} \cdot e^{\frac{-\tau}{\tau_{\text{proper}}}}, \quad (3.27)$$

and the inverse distribution that was sampled from

$$\text{PDF}_{\text{inv}} = \frac{1}{\tau \cdot (\ln(\tau_{\max}) - \ln(\tau_{\min}))}. \quad (3.28)$$

This re-weighting factor is then calculated as

$$w_{\text{lifetime}} = \frac{\text{PDF}_{\text{exp}}}{\text{PDF}_{\text{inv}}} = \frac{\Gamma_{\text{total}}(m_4) \cdot |U_{\tau 4}|^2}{\hbar} \cdot \tau \cdot (\ln(\tau_{\max}) - \ln(\tau_{\min})) \cdot e^{\frac{-\tau}{\tau_{\text{proper}}}}. \quad (3.29)$$

Adding another factor of $|U_{\tau 4}|^2$ to account for the mixing at the interaction vertex the total re-weighting factor becomes

$$w_{\text{total}} = |U_{\tau 4}|^2 \cdot w_{\text{lifetime}}. \quad (3.30)$$

If this additional weighting factor is multiplied to a generation weight with units m^2 (like in Equation 3.31), the livetime in s , and the oscillated primary neutrino flux in $\text{m}^{-2}\text{s}^{-1}$, it results in the number of expected events in the detector for this particular MC event for a chosen mixing (and mass).

3.3 Background Simulation

The MC is used in the analysis by applying a method called *forward folding*, where a very large number of events (signal and background) is produced using sampling distribution that are tuned to have a large selection efficiency. Those distributions don't have to be physically correct distributions, but they need to cover the full parameter space of interest for the analysis. To produce a physical distribution, the events are weighted given a specific choice of physics and nuisance parameters. The large number of raw MC events ensures a good estimation of the expected numbers and weighted distributions.

The analysis itself is then performed by comparing the weighted MC distributions to the observed data. This is done by binning them as described in Chapter ?? and calculating a loss function comparing the bin expectations to

Flavor	Energy [GeV]	Radius [m]	Length [m]	Events/File	Files
$\nu_e + \bar{\nu}_e$	1-4			450000	
	4-12	250	500		
	12-100	350	600	100000	650
$\nu_\mu + \bar{\nu}_\mu$	100-10000	550	1000	57500	
	1-5	250	500	408000	
	5-80	400	900	440000	
$\nu_\tau + \bar{\nu}_\tau$	80-1000	450		57500	1550
	1000-10000	550	1500	6700	
	1-4			1500000	
$\nu_\tau + \bar{\nu}_\tau$	4-10	250	500	300000	
	10-50	350	600	375000	350
	50-1000	450	800	200000	
	1000-10000	550	1500	26000	

Table 3.5: Cylinder volumes used for GENIE neutrino simulation generation. Cylinder is always centered in DeepCore at $(x, y, z) = (46.29, -34.88, -330.00)$ m.

the data. The physics and nuisance parameters that best correspond to the observed data are estimated by minimizing this loss function. In order to achieve a reliable result with this method the MC needs to be precise and as close to the data as possible (at least at the final event selection).

3.3.1 Neutrinos

Due to the very low interaction rate of neutrinos, the event generation is performed in a way that forces every event to interact in a chosen sampling volume. The weight of each event is then calculated as the inverse of the simulated neutrino fluence

$$w_{\text{gen}} = \frac{1}{F_{\text{sim}}} \frac{1}{N_{\text{sim}}} , \quad (3.31)$$

where F_{sim} is the number of neutrino events per energy, time, area, and solid angle and N_{sim} is the number of simulated events. If this weight is multiplied by the livetime and the theoretically expected neutrino flux for a given physical model, it results in the number of expected events in the detector for this particular MC event. The baseline neutrino flux used in this thesis, computed for the South Pole, is taken from Honda *et al.* [75].

The simulation volume is a cylinder centered in DeepCore with radius and height chosen such that all events possibly producing a signal are contained. The different sizes, chosen depending on energy and neutrino flavor, are shown in Table 3.5. The directions of the neutrinos are sampled isotropically and the energies are sampled from an E^{-2} power law. The number of simulated events is chosen such that the livetime is more than 70 years for each flavor. Neutrinos and antineutrinos are simulated with ratios of 70% and 30%, respectively.

To simulate the neutrino interaction with the ice, the GENIE event generator [92] (version 2.12.8) is used, resulting in the secondary particles and the kinematic and cross-section parameters. As input, the outdated GRV98LO [93] *parton distribution functions (PDFs)* was used, because it was the only option that could incorporate extrapolations to lower Q^2 [94]. Muons produced in these interactions are propagated using PROPOSAL [95], also simulating their

[75]: Honda et al. (2015), “Atmospheric neutrino flux calculation using the NRLMSISE-00 atmospheric model”

[92]: Andreopoulos et al. (2015), “The GENIE Neutrino Monte Carlo Generator: Physics and User Manual”

[93]: Glück et al. (1998), “Dynamical parton distributions revisited”

[94]: Bodek et al. (2003), “Higher twist, xi(omega) scaling, and effective LO PDFs for lepton scattering in the few GeV region”

[95]: Koehne et al. (2013), “PROPOSAL: A tool for propagation of charged leptons”

[83]: Agostinelli et al. (2003), “Geant4—a simulation toolkit”

[84]: Rädel et al. (2012), “Calculation of the Cherenkov light yield from low energetic secondary particles accompanying high-energy muons in ice and water with Geant4 simulations”

[96]: Becherini et al. (2006), “A parameterisation of single and multiple muons in the deep water or ice”

[97]: Heck et al. (1998), “CORSIKA: A Monte Carlo code to simulate extensive air showers”

[98]: Gaisser (2012), “Spectrum of cosmic-ray nucleons, kaon production, and the atmospheric muon charge ratio”

[99]: Engel et al. (2017), “The hadronic interaction model Sibyll – past, present and future”

Cherenkov light output. The shower development of gamma rays, electrons, and positrons below 100 MeV and hadronic showers below 30 GeV is simulated using Geant4 [83] while for higher energies an analytical approximation from [84] is used.

3.3.2 Muons

Atmospheric muons are generated on a cylinder surface enclosing the full IceCube detector array. The cylinder has a height of 1600 m and a radius of 800 m. The energy is sampled from an E^{-3} power law while the other sampling distributions (position, direction) are found from parameterizations based on [96]. This work uses full CORSIKA [97] simulations of muons to tailor the parameterizations, starting from *cosmic ray* (CR) interactions with atmospheric nuclei using the CR flux model from [98] and producing the muons applying the *hadronic interaction* (HI) model SIBYLL 2.1 [99]. After the generation, they are propagated through the ice with PROPOSAL producing photons, treating them exactly like the muons produced in neutrino interactions.

Since the offline processing and selection steps described in Section ?? and Section ?? reduce the muon contamination to an almost negligible level, the statistical uncertainty on the number of expected muon events at the final selection level is large and therefore two separate sets of muon simulation are produced. **A first set** including all events resulting from the above described generation to tune the lower level selection (up to L4) and **a second set** to estimate the muon contamination at higher levels (above L5), which only accepts muon events if they pass through a smaller cylinder centered in DeepCore (height of 400 m and radius of 180 m) and rejects events based on a KDE estimated muon density at L5 (in energy and zenith) increasing the simulation efficiency at L5 significantly.

APPENDIX

A

Heavy Neutral Lepton Event Generation

A.1 Model-Independent Simulation Distributions

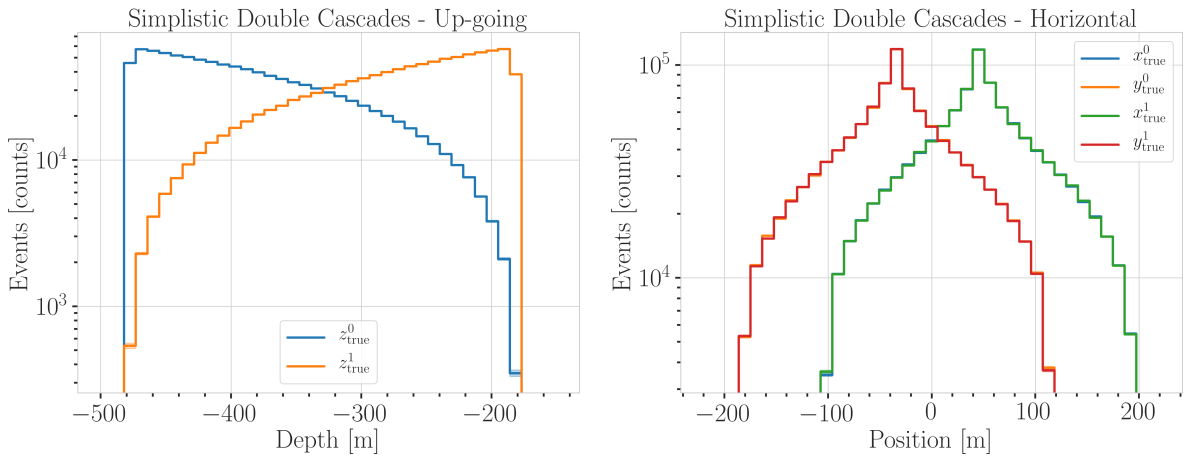


Figure A.1: Generation level distributions of the simplistic simulation sets. Vertical positions of the cascades in the up-going sample (left) and horizontal positions of the cascades in the horizontal sample (right).

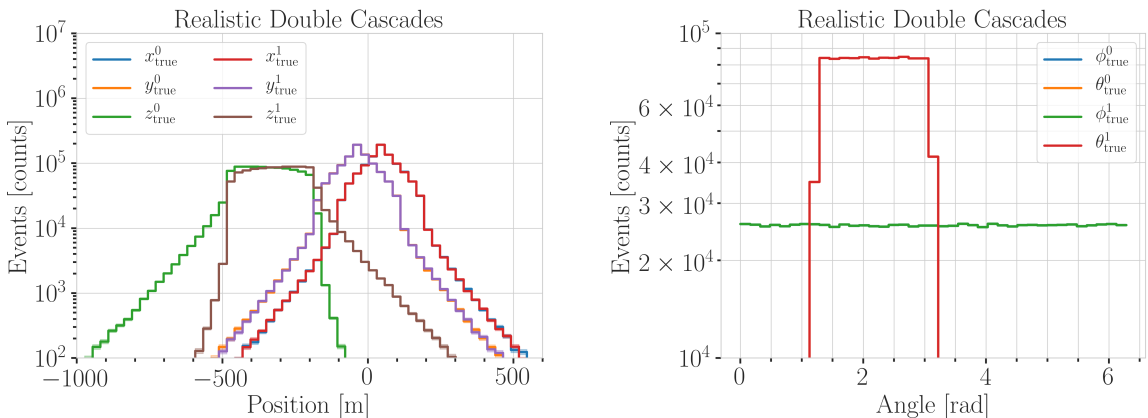


Figure A.2: Generation level distributions of the realistic simulation set. Shown are the cascade x, y, z positions (left) and the cascade direction angles (right).

A.2 Model-Dependent Simulation Distributions

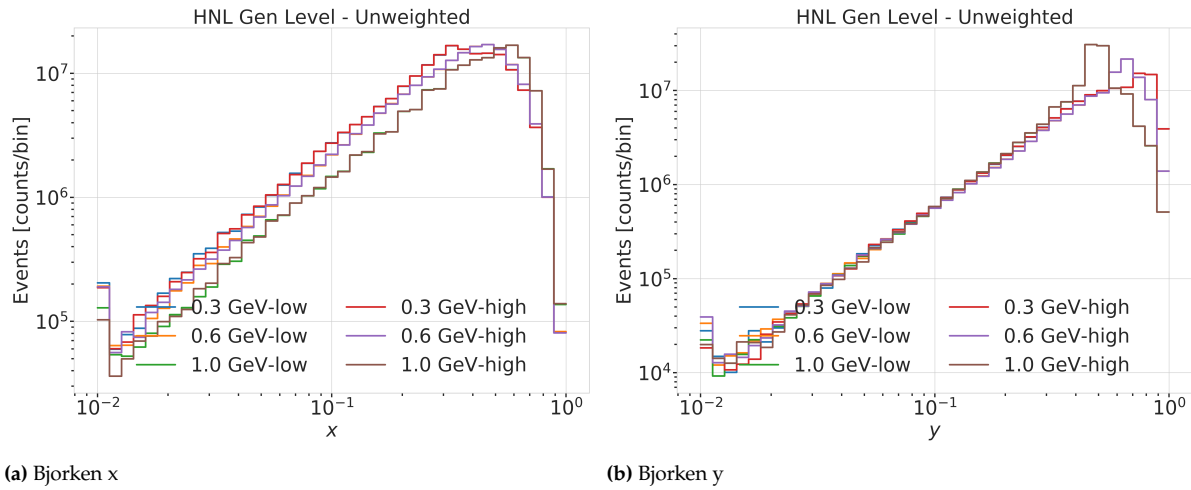


Figure A.3: Generation level distributions of the model dependent simulation.

B

Analysis Results

B.1 Final Level Simulation Distributions

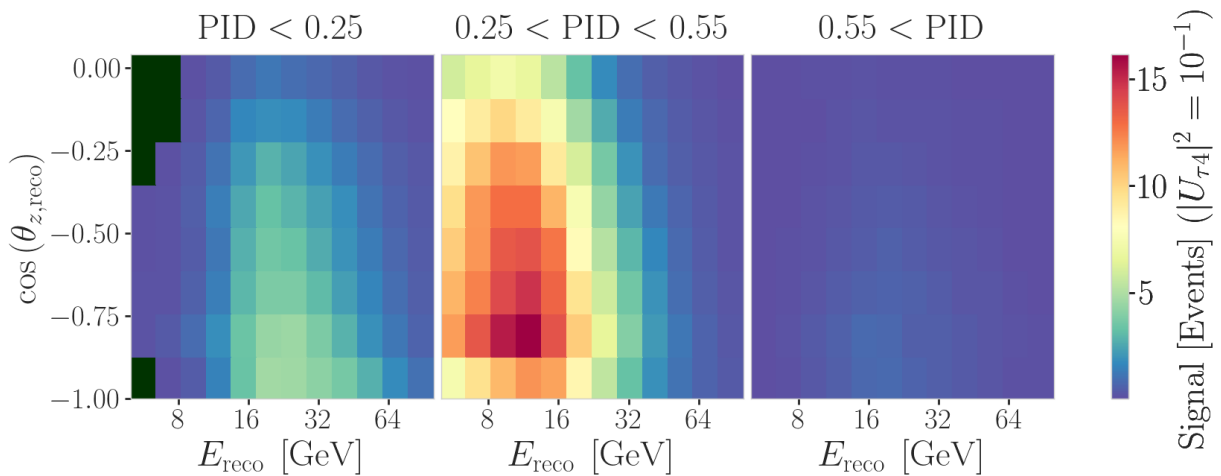


Figure B.1: Signal expectation in 9.28 years for the 1.0 GeV mass sample at a mixing of 0.1, while all other parameters are at their nominal values (top) and observed data (bottom).

B.2 Treatment of Detector Systematic Uncertainties

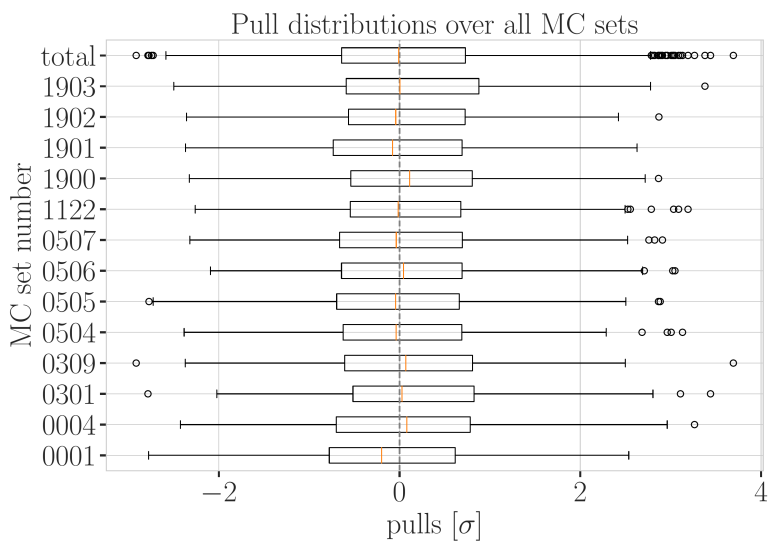


Figure B.2: Overall performance of the detector systematic uncertainty treatment. Shown are the pull distributions of the three dimensional pulls shown in Figure ?? and Figure B.3 between the nominal set and the specific systematic set, after the nominal set was re-weighted to the corresponding systematic parameter value.

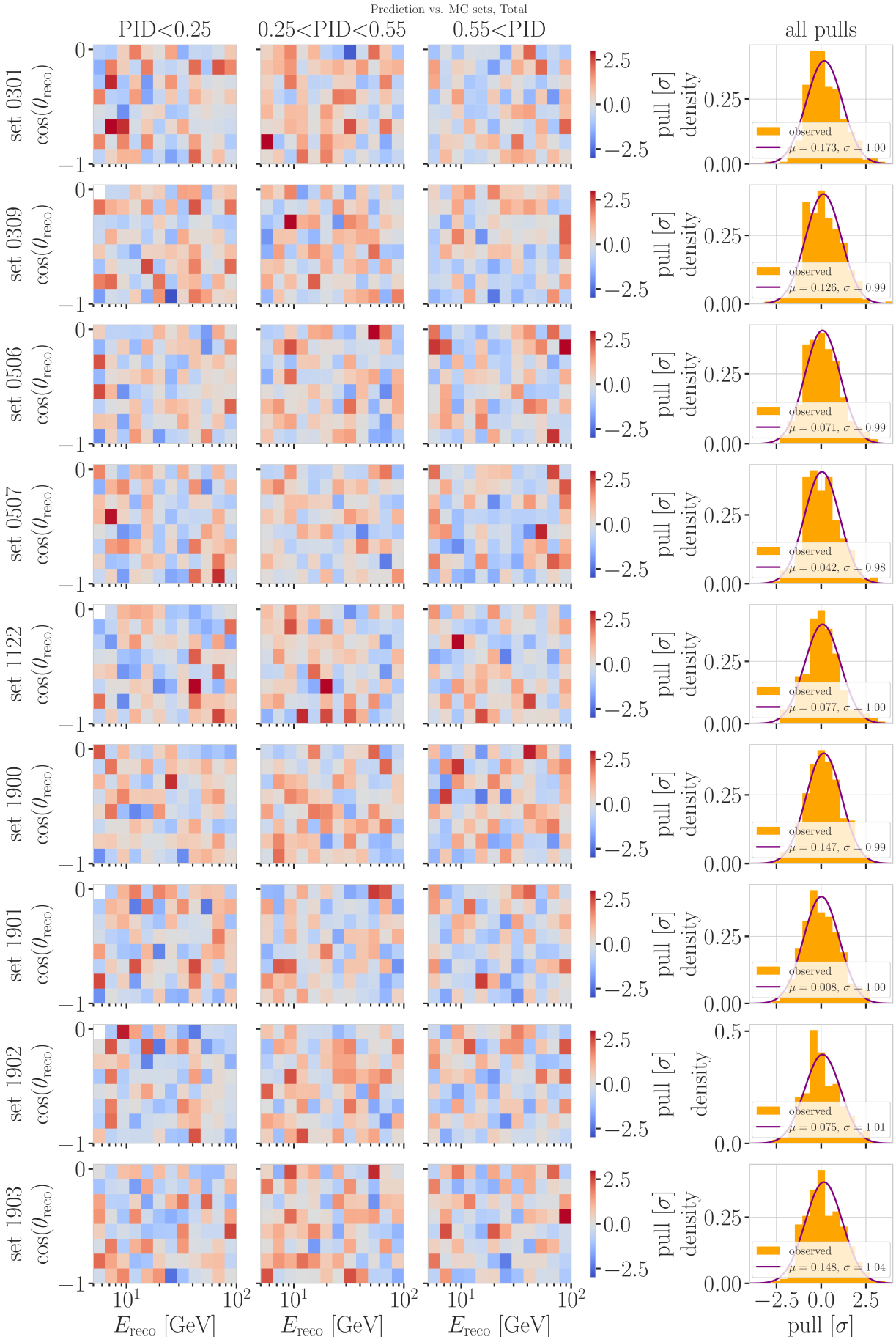


Figure B.3: Three dimensional pulls and set-wise pull distributions between the nominal set and the specific systematic sets, after the nominal set was re-weighted to the corresponding systematic parameter value.

B.3 Best Fit Nuisance Parameters

Table B.1: Best fit nuisance parameters for the three mass samples. Also shown is the nominal value and the difference between the nominal and the best fit.

Parameter	Nominal	Best Fit			Nominal - Best Fit		
		0.3 GeV	0.6 GeV	1.0 GeV	0.3 GeV	0.6 GeV	1.0 GeV
$ U_{\tau 4} ^2$	-	0.003019	0.080494	0.106141	-	-	-
$\theta_{23}[\circ]$	47.5047	48.117185	47.918758	48.010986	-0.612485	-0.414058	-0.506286
$\Delta m_{31}^2 [\text{eV}^2]$	0.002475	0.002454	0.002454	0.002455	0.000020	0.000021	0.000019
N_ν	1.0	0.889149	0.889055	0.889559	0.110851	0.110945	0.110441
$\Delta \gamma_\nu$	0.0	-0.007926	-0.006692	-0.006596	0.007926	0.006692	0.006596
Barr h_{π^+}	0.0	-0.147475	-0.148481	-0.148059	0.147475	0.148481	0.148059
Barr i_{π^+}	0.0	0.475448	0.513393	0.521626	-0.475448	-0.513393	-0.521626
Barr y_{K^+}	0.0	0.076176	0.062893	0.057548	-0.076176	-0.062893	-0.057548
DIS	0.0	-0.248709	-0.223302	-0.215666	0.248709	0.223302	0.215666
$M_{A,\text{QE}}$	0.0	-0.170528	-0.128150	-0.120345	0.170528	0.128150	0.120345
$M_{A,\text{res}}$	0.0	-0.125855	-0.080875	-0.070716	0.125855	0.080875	0.070716
ϵ_{DOM}	1.0	1.021984	1.017789	1.016689	-0.021984	-0.017789	-0.016689
hole ice p_0	0.101569	-0.161341	-0.161051	-0.160129	0.262910	0.262620	0.261698
hole ice p_1	-0.049344	-0.073701	-0.075596	-0.076261	0.024357	0.026252	0.026917
ice absorption	1.00	0.943261	0.942463	0.942000	0.056739	0.057537	0.058000
ice scattering	1.05	0.986152	0.989289	0.989438	0.063848	0.060711	0.060562
N_{bfr}	0.0	0.746684	0.740255	0.736215	-0.746684	-0.740255	-0.736215

fix design + significant
digits to show (OR-
ANGE)

maybe show range/prior
and then deviation in
sigma, or absolute for the
ones without prior

Bibliography

Here are the references in citation order.

- [1] W. Pauli. "Dear radioactive ladies and gentlemen". In: *Phys. Today* 31N9 (1978), p. 27 (cited on page 2).
- [2] C. L. Cowan et al. "Detection of the Free Neutrino: a Confirmation". In: *Science* 124.3212 (1956), pp. 103–104. doi: [10.1126/science.124.3212.103](https://doi.org/10.1126/science.124.3212.103) (cited on page 2).
- [3] G. Danby et al. "Observation of High-Energy Neutrino Reactions and the Existence of Two Kinds of Neutrinos". In: *Phys. Rev. Lett.* 9 (1 July 1962), pp. 36–44. doi: [10.1103/PhysRevLett.9.36](https://doi.org/10.1103/PhysRevLett.9.36) (cited on page 2).
- [4] K. Kodama et al. "Observation of tau neutrino interactions". In: *Physics Letters B* 504.3 (2001), pp. 218–224. doi: [https://doi.org/10.1016/S0370-2693\(01\)00307-0](https://doi.org/10.1016/S0370-2693(01)00307-0) (cited on page 2).
- [5] R. Davis, D. S. Harmer, and K. C. Hoffman. "Search for Neutrinos from the Sun". In: *Phys. Rev. Lett.* 20 (21 May 1968), pp. 1205–1209. doi: [10.1103/PhysRevLett.20.1205](https://doi.org/10.1103/PhysRevLett.20.1205) (cited on pages 2, 8).
- [6] M. G. Aartsen et al. "The IceCube Neutrino Observatory: instrumentation and online systems". In: *Journal of Instrumentation* 12.3 (Mar. 2017), P03012. doi: [10.1088/1748-0221/12/03/P03012](https://doi.org/10.1088/1748-0221/12/03/P03012) (cited on page 2).
- [7] C. N. Yang and R. L. Mills. "Conservation of Isotopic Spin and Isotopic Gauge Invariance". In: *Physical Review* 96.1 (Oct. 1954), pp. 191–195. doi: [10.1103/PhysRev.96.191](https://doi.org/10.1103/PhysRev.96.191) (cited on page 5).
- [8] S. Weinberg. "A Model of Leptons". In: *Phys. Rev. Lett.* 19 (21 Nov. 1967), pp. 1264–1266. doi: [10.1103/PhysRevLett.19.1264](https://doi.org/10.1103/PhysRevLett.19.1264) (cited on page 5).
- [9] S. L. Glashow. "Partial-symmetries of weak interactions". In: *Nuclear Physics* 22.4 (Feb. 1961), pp. 579–588. doi: [10.1016/0029-5582\(61\)90469-2](https://doi.org/10.1016/0029-5582(61)90469-2) (cited on page 5).
- [10] R. Jackiw. "Physical Formulations: Elementary Particle Theory. Relativistic Groups and Analyticity. Proceedings of the eighth Nobel Symposium, Aspenäsgården, Lerum, Sweden, May 1968. Nils Svartholm, Ed. Interscience (Wiley), New York, and Almqvist and Wiksell, Stockholm, 1969. 400 pp., illus. \$31.75." In: *Science* 168.3936 (1970), pp. 1196–1197. doi: [10.1126/science.168.3936.1196.b](https://doi.org/10.1126/science.168.3936.1196.b) (cited on page 5).
- [11] P. Higgs. "Broken symmetries, massless particles and gauge fields". In: *Physics Letters* 12.2 (1964), pp. 132–133. doi: [https://doi.org/10.1016/0031-9163\(64\)91136-9](https://doi.org/10.1016/0031-9163(64)91136-9) (cited on page 5).
- [12] S. Chatrchyan et al. "Observation of a New Boson at a Mass of 125 GeV with the CMS Experiment at the LHC". In: *Phys. Lett. B* 716 (2012), pp. 30–61. doi: [10.1016/j.physletb.2012.08.021](https://doi.org/10.1016/j.physletb.2012.08.021) (cited on page 5).
- [13] G. Aad et al. "Observation of a new particle in the search for the Standard Model Higgs boson with the ATLAS detector at the LHC". In: *Phys. Lett. B* 716 (2012), pp. 1–29. doi: [10.1016/j.physletb.2012.08.020](https://doi.org/10.1016/j.physletb.2012.08.020) (cited on page 5).
- [14] M. Gell-Mann. "A Schematic Model of Baryons and Mesons". In: *Resonance* 24 (1964), pp. 923–925 (cited on page 5).
- [15] G. Zweig. "An SU(3) model for strong interaction symmetry and its breaking. Version 2". In: *DEVELOPMENTS IN THE QUARK THEORY OF HADRONS. VOL. 1. 1964 - 1978*. Ed. by D. B. Lichtenberg and S. P. Rosen. Feb. 1964, pp. 22–101 (cited on page 5).
- [16] D. J. Gross and F. Wilczek. "Ultraviolet Behavior of Non-Abelian Gauge Theories". In: *PRL* 30.26 (June 1973), pp. 1343–1346. doi: [10.1103/PhysRevLett.30.1343](https://doi.org/10.1103/PhysRevLett.30.1343) (cited on page 5).
- [17] C. Giunti and C. W. Kim. *Fundamentals of Neutrino Physics and Astrophysics*. Oxford University Press, Mar. 2007 (cited on page 5).

- [18] M. D. Schwartz. *Quantum Field Theory and the Standard Model*. Cambridge University Press, 2013 (cited on page 5).
- [19] A. Trettin. "Search for eV-scale sterile neutrinos with IceCube DeepCore". PhD thesis. Berlin, Germany: Humboldt-Universität zu Berlin, Mathematisch-Naturwissenschaftliche Fakultät, 2023. doi: <https://github.com/atrettin/PhD-Thesis> (cited on pages 7, 10).
- [20] N. Deruelle, J.-P. Uzan, and P. de Forcrand-Millard. *Relativity in Modern Physics*. Oxford University Press, Aug. 2018 (cited on page 8).
- [21] R. L. Workman et al. "Review of Particle Physics". In: *Progress of Theoretical and Experimental Physics* 2022.8 (Aug. 2022), p. 083C01. doi: [10.1093/ptep/ptac097](https://doi.org/10.1093/ptep/ptac097) (cited on pages 8, 29).
- [22] M. Fukugita and T. Yanagida. "Baryogenesis without grand unification". In: *Physics Letters B* 174.1 (1986), pp. 45–47. doi: [https://doi.org/10.1016/0370-2693\(86\)91126-3](https://doi.org/10.1016/0370-2693(86)91126-3) (cited on page 8).
- [23] Y. Fukuda et al. "Evidence for Oscillation of Atmospheric Neutrinos". In: *Phys. Rev. Lett.* 81 (8 Aug. 1998), pp. 1562–1567. doi: [10.1103/PhysRevLett.81.1562](https://doi.org/10.1103/PhysRevLett.81.1562) (cited on page 8).
- [24] Q. R. Ahmad and other. "Direct Evidence for Neutrino Flavor Transformation from Neutral-Current Interactions in the Sudbury Neutrino Observatory". In: *Phys. Rev. Lett.* 89 (1 June 2002), p. 011301. doi: [10.1103/PhysRevLett.89.011301](https://doi.org/10.1103/PhysRevLett.89.011301) (cited on page 8).
- [25] S. Alam et al. "Completed SDSS-IV extended Baryon Oscillation Spectroscopic Survey: Cosmological implications from two decades of spectroscopic surveys at the Apache Point Observatory". In: *Phys. Rev. D* 103 (8 Apr. 2021), p. 083533. doi: [10.1103/PhysRevD.103.083533](https://doi.org/10.1103/PhysRevD.103.083533) (cited on page 8).
- [26] N. Aghanim et al. "Planck2018 results: VI. Cosmological parameters". In: *Astronomy & Astrophysics* 641 (Sept. 2020), A6. doi: [10.1051/0004-6361/201833910](https://doi.org/10.1051/0004-6361/201833910) (cited on page 8).
- [27] M. Aker et al. "Direct neutrino-mass measurement with sub-electronvolt sensitivity". In: *Nature Phys.* 18.2 (2022), pp. 160–166. doi: [10.1038/s41567-021-01463-1](https://doi.org/10.1038/s41567-021-01463-1) (cited on page 8).
- [28] T. Asaka, S. Blanchet, and M. Shaposhnikov. "The nuMSM, dark matter and neutrino masses". In: *Phys. Lett. B* 631 (2005), pp. 151–156. doi: [10.1016/j.physletb.2005.09.070](https://doi.org/10.1016/j.physletb.2005.09.070) (cited on page 10).
- [29] T. Asaka and M. Shaposhnikov. "The νMSM, dark matter and baryon asymmetry of the universe". In: *Phys. Lett. B* 620 (2005), pp. 17–26. doi: [10.1016/j.physletb.2005.06.020](https://doi.org/10.1016/j.physletb.2005.06.020) (cited on page 10).
- [30] P. Minkowski. " $\mu \rightarrow e \gamma$ at a rate of one out of 10^9 muon decays?" In: *Physics Letters B* 67.4 (Apr. 1977), pp. 421–428. doi: [10.1016/0370-2693\(77\)90435-X](https://doi.org/10.1016/0370-2693(77)90435-X) (cited on page 10).
- [31] T. Yanagida. "Horizontal Symmetry and Masses of Neutrinos". In: *Progress of Theoretical Physics* 64.3 (Sept. 1980), pp. 1103–1105. doi: [10.1143/PTP.64.1103](https://doi.org/10.1143/PTP.64.1103) (cited on page 10).
- [32] S. L. Glashow. "The Future of Elementary Particle Physics". In: *NATO Sci. Ser. B* 61 (1980), p. 687. doi: [10.1007/978-1-4684-7197-7_15](https://doi.org/10.1007/978-1-4684-7197-7_15) (cited on page 10).
- [33] M. Gell-Mann, P. Ramond, and R. Slansky. "Complex Spinors and Unified Theories". In: *Conf. Proc. C* 790927 (1979), pp. 315–321 (cited on page 10).
- [34] R. N. Mohapatra and G. Senjanović. "Neutrino Mass and Spontaneous Parity Nonconservation". In: *Phys. Rev. Lett.* 44 (14 Apr. 1980), pp. 912–915. doi: [10.1103/PhysRevLett.44.912](https://doi.org/10.1103/PhysRevLett.44.912) (cited on page 10).
- [35] M. G. Aartsen et al. "eV-Scale Sterile Neutrino Search Using Eight Years of Atmospheric Muon Neutrino Data from the IceCube Neutrino Observatory". In: *Phys. Rev. Lett.* 125.14 (2020), p. 141801. doi: [10.1103/PhysRevLett.125.141801](https://doi.org/10.1103/PhysRevLett.125.141801) (cited on page 10).
- [36] J.-L. Tastet, O. Ruchayskiy, and I. Timiryasov. "Reinterpreting the ATLAS bounds on heavy neutral leptons in a realistic neutrino oscillation model". In: *JHEP* 12 (2021), p. 182. doi: [10.1007/JHEP12\(2021\)182](https://doi.org/10.1007/JHEP12(2021)182) (cited on page 11).
- [37] D. A. Bryman and R. Shrock. "Constraints on Sterile Neutrinos in the MeV to GeV Mass Range". In: *Phys. Rev. D* 100 (2019), p. 073011. doi: [10.1103/PhysRevD.100.073011](https://doi.org/10.1103/PhysRevD.100.073011) (cited on pages 11, 12).
- [38] A. Aguilar-Arevalo et al. "Improved search for heavy neutrinos in the decay $\pi \rightarrow ev$ ". In: *Phys. Rev. D* 97.7 (2018), p. 072012. doi: [10.1103/PhysRevD.97.072012](https://doi.org/10.1103/PhysRevD.97.072012) (cited on page 11).

- [39] G. Bellini et al. "New limits on heavy sterile neutrino mixing in B8 decay obtained with the Borexino detector". In: *Phys. Rev. D* 88.7 (2013), p. 072010. doi: [10.1103/PhysRevD.88.072010](https://doi.org/10.1103/PhysRevD.88.072010) (cited on pages 11, 14).
- [40] D. Britton et al. "Improved search for massive neutrinos in $\pi^+ \rightarrow e^+ \nu$ decay". In: *Physical Review D* 46 (1992) (cited on page 11).
- [41] C. J. Parkinson et al. "Search for heavy neutral lepton production at the NA62 experiment". In: *PoS EPS-HEP2021* (2022), p. 686. doi: [10.22323/1.398.0686](https://doi.org/10.22323/1.398.0686) (cited on pages 11, 12).
- [42] K. Abe et al. "Search for heavy neutrinos with the T2K near detector ND280". In: *Phys. Rev. D* 100.5 (2019), p. 052006. doi: [10.1103/PhysRevD.100.052006](https://doi.org/10.1103/PhysRevD.100.052006) (cited on pages 11, 12).
- [43] P. Abreu et al. "Search for neutral heavy leptons produced in Z decays". In: *Z. Phys. C* 74 (1997). [Erratum: *Z.Phys.C* 75, 580 (1997)], pp. 57–71. doi: [10.1007/s002880050370](https://doi.org/10.1007/s002880050370) (cited on pages 11, 13).
- [44] R. Barouki, G. Marocco, and S. Sarkar. "Blast from the past II: Constraints on heavy neutral leptons from the BEBC WA66 beam dump experiment". In: *SciPost Phys.* 13 (2022), p. 118. doi: [10.21468/SciPostPhys.13.5.118](https://doi.org/10.21468/SciPostPhys.13.5.118) (cited on pages 11–13).
- [45] F. Bergsma et al. "A Search for Decays of Heavy Neutrinos". In: *Phys. Lett. B* 128 (1983). Ed. by J. Tran Thanh Van, p. 361. doi: [10.1016/0370-2693\(83\)90275-7](https://doi.org/10.1016/0370-2693(83)90275-7) (cited on page 11).
- [46] G. Aad et al. "Search for heavy neutral leptons in decays of W bosons produced in 13 TeV pp collisions using prompt and displaced signatures with the ATLAS detector". In: *JHEP* 10 (2019), p. 265. doi: [10.1007/JHEP10\(2019\)265](https://doi.org/10.1007/JHEP10(2019)265) (cited on pages 11, 12).
- [47] G. Aad et al. "Search for Heavy Neutral Leptons in Decays of W Bosons Using a Dilepton Displaced Vertex in $\sqrt{s} = 13\text{TeV}$ pp Collisions with the ATLAS Detector". In: *Phys. Rev. Lett.* 131 (6 Aug. 2023), p. 061803. doi: [10.1103/PhysRevLett.131.061803](https://doi.org/10.1103/PhysRevLett.131.061803) (cited on pages 11, 12).
- [48] A. M. Sirunyan et al. "Search for heavy neutral leptons in events with three charged leptons in proton-proton collisions at $\sqrt{s} = 13\text{ TeV}$ ". In: *Phys. Rev. Lett.* 120.22 (2018), p. 221801. doi: [10.1103/PhysRevLett.120.221801](https://doi.org/10.1103/PhysRevLett.120.221801) (cited on pages 11, 12).
- [49] A. Tumasyan et al. "Search for long-lived heavy neutral leptons with displaced vertices in proton-proton collisions at $\sqrt{s} = 13\text{ TeV}$ ". In: *JHEP* 07 (2022), p. 081. doi: [10.1007/JHEP07\(2022\)081](https://doi.org/10.1007/JHEP07(2022)081) (cited on pages 11, 12).
- [50] A. Vaitaitis et al. "Search for neutral heavy leptons in a high-energy neutrino beam". In: *Phys. Rev. Lett.* 83 (1999), pp. 4943–4946. doi: [10.1103/PhysRevLett.83.4943](https://doi.org/10.1103/PhysRevLett.83.4943) (cited on pages 11, 12).
- [51] E. Fernandez-Martinez et al. "Effective portals to heavy neutral leptons". In: *JHEP* 09 (2023), p. 001. doi: [10.1007/JHEP09\(2023\)001](https://doi.org/10.1007/JHEP09(2023)001) (cited on pages 11–13).
- [52] G. Bernardi et al. "Search for Neutrino Decay". In: *Phys. Lett. B* 166 (1986), pp. 479–483. doi: [10.1016/0370-2693\(86\)91602-3](https://doi.org/10.1016/0370-2693(86)91602-3) (cited on page 11).
- [53] S. Ito et al. "Search for heavy neutrinos in $\pi^+ \rightarrow \mu^+ \nu$ decay and status of lepton universality test in the PIENU experiment". In: *JPS Conf. Proc.* 33 (2021). Ed. by N. Saito, pp. 011131-1–011131-6. doi: [10.7566/JPSCP.33.011131](https://doi.org/10.7566/JPSCP.33.011131) (cited on page 11).
- [54] A. V. Artamonov et al. "Search for heavy neutrinos in $K^+ \rightarrow \mu^+ \nu_H$ decays". In: *Phys. Rev. D* 91.5 (2015). [Erratum: *Phys.Rev.D* 91, 059903 (2015)], p. 052001. doi: [10.1103/PhysRevD.91.052001](https://doi.org/10.1103/PhysRevD.91.052001) (cited on pages 11, 12).
- [55] P. Abratenko et al. "Search for Heavy Neutral Leptons in Electron-Positron and Neutral-Pion Final States with the MicroBooNE Detector". In: *Phys. Rev. Lett.* 132.4 (2024), p. 041801. doi: [10.1103/PhysRevLett.132.041801](https://doi.org/10.1103/PhysRevLett.132.041801) (cited on pages 11, 12).
- [56] P. Astier et al. "Search for heavy neutrinos mixing with tau neutrinos". In: *Phys. Lett. B* 506 (2001), pp. 27–38. doi: [10.1016/S0370-2693\(01\)00362-8](https://doi.org/10.1016/S0370-2693(01)00362-8) (cited on page 12).
- [57] J. Orloff, A. N. Rozanov, and C. Santoni. "Limits on the mixing of tau neutrino to heavy neutrinos". In: *Phys. Lett. B* 550 (2002), pp. 8–15. doi: [10.1016/S0370-2693\(02\)02769-7](https://doi.org/10.1016/S0370-2693(02)02769-7) (cited on pages 12, 13).

- [58] I. Boiarska et al. "Constraints from the CHARM experiment on heavy neutral leptons with tau mixing". In: *Phys. Rev. D* 104.9 (2021), p. 095019. doi: [10.1103/PhysRevD.104.095019](https://doi.org/10.1103/PhysRevD.104.095019) (cited on pages 12, 13).
- [59] A. Cooper-Sarkar et al. "Search for heavy neutrino decays in the BEBC beam dump experiment". In: *Physics Letters B* 160.1 (1985), pp. 207–211. doi: [https://doi.org/10.1016/0370-2693\(85\)91493-5](https://doi.org/10.1016/0370-2693(85)91493-5) (cited on page 12).
- [60] B. Shuve and M. E. Peskin. "Revision of the LHCb Limit on Majorana Neutrinos". In: *Phys. Rev. D* 94.11 (2016), p. 113007. doi: [10.1103/PhysRevD.94.113007](https://doi.org/10.1103/PhysRevD.94.113007) (cited on page 12).
- [61] R. Aaij et al. "Search for heavy neutral leptons in $W^+ \rightarrow \mu^+ \mu^\pm$ jet decays". In: *Eur. Phys. J. C* 81.3 (2021), p. 248. doi: [10.1140/epjc/s10052-021-08973-5](https://doi.org/10.1140/epjc/s10052-021-08973-5) (cited on pages 12, 13).
- [62] R. Plestid. "Luminous solar neutrinos I: Dipole portals". In: *Phys. Rev. D* 104 (2021), p. 075027. doi: [10.1103/PhysRevD.104.075027](https://doi.org/10.1103/PhysRevD.104.075027) (cited on pages 13, 14).
- [63] A. Osipowicz et al. "KATRIN: A Next generation tritium beta decay experiment with sub-eV sensitivity for the electron neutrino mass. Letter of intent". In: (Sept. 2001) (cited on page 13).
- [64] S. Mertens et al. "A novel detector system for KATRIN to search for keV-scale sterile neutrinos". In: *Journal of Physics G: Nuclear and Particle Physics* 46.6 (2019), p. 065203. doi: [10.1088/1361-6471/ab12fe](https://doi.org/10.1088/1361-6471/ab12fe) (cited on page 13).
- [65] M. Aker et al. "Search for keV-scale sterile neutrinos with the first KATRIN data". In: *Eur. Phys. J. C* 83.8 (2023), p. 763. doi: [10.1140/epjc/s10052-023-11818-y](https://doi.org/10.1140/epjc/s10052-023-11818-y) (cited on page 13).
- [66] B. Abi et al. "Deep Underground Neutrino Experiment (DUNE), Far Detector Technical Design Report, Volume II: DUNE Physics". In: (Feb. 2020) (cited on page 13).
- [67] S. Friedrich et al. "Limits on the Existence of sub-MeV Sterile Neutrinos from the Decay of ${}^7\text{Be}$ in Superconducting Quantum Sensors". In: *Phys. Rev. Lett.* 126.2 (2021), p. 021803. doi: [10.1103/PhysRevLett.126.021803](https://doi.org/10.1103/PhysRevLett.126.021803) (cited on page 13).
- [68] C. Hagner et al. "Experimental search for the neutrino decay $\nu_3 + \nu_j + e^+ + e^-$ and limits on neutrino mixing". English. In: 52.3 (1995), pp. 1343–1352. doi: [10.1103/PhysRevD.52.1343](https://doi.org/10.1103/PhysRevD.52.1343) (cited on page 14).
- [69] R. Plestid. "Luminous solar neutrinos II: Mass-mixing portals". In: *Phys. Rev. D* 104 (2021). [Erratum: *Phys. Rev. D* 105, 099901 (2022)], p. 075028. doi: [10.1103/PhysRevD.104.075028](https://doi.org/10.1103/PhysRevD.104.075028) (cited on page 14).
- [70] P. Coloma et al. "Double-Cascade Events from New Physics in Icecube". In: *Phys. Rev. Lett.* 119.20 (2017), p. 201804. doi: [10.1103/PhysRevLett.119.201804](https://doi.org/10.1103/PhysRevLett.119.201804) (cited on page 14).
- [71] P. Coloma. "Icecube/DeepCore tests for novel explanations of the MiniBooNE anomaly". In: *Eur. Phys. J. C* 79.9 (2019), p. 748. doi: [10.1140/epjc/s10052-019-7256-8](https://doi.org/10.1140/epjc/s10052-019-7256-8) (cited on page 14).
- [72] M. Atkinson et al. "Heavy Neutrino Searches through Double-Bang Events at Super-Kamiokande, DUNE, and Hyper-Kamiokande". In: *JHEP* 04 (2022), p. 174. doi: [10.1007/JHEP04\(2022\)174](https://doi.org/10.1007/JHEP04(2022)174) (cited on page 14).
- [73] P. Coloma et al. "GeV-scale neutrinos: interactions with mesons and DUNE sensitivity". In: *Eur. Phys. J. C* 81.1 (2021), p. 78. doi: [10.1140/epjc/s10052-021-08861-y](https://doi.org/10.1140/epjc/s10052-021-08861-y) (cited on pages 14, 20, 26, 28, 30).
- [74] M. Tanabashi et al. "Review of Particle Physics". In: *Phys. Rev. D* 98 (3 Aug. 2018), p. 030001. doi: [10.1103/PhysRevD.98.030001](https://doi.org/10.1103/PhysRevD.98.030001) (cited on pages 15, 17).
- [75] M. Honda et al. "Atmospheric neutrino flux calculation using the NRLMSISE-00 atmospheric model". In: *Phys. Rev. D* 92 (2 July 2015), p. 023004. doi: [10.1103/PhysRevD.92.023004](https://doi.org/10.1103/PhysRevD.92.023004) (cited on pages 15, 33).
- [76] A. Fedynitch et al. "Calculation of conventional and prompt lepton fluxes at very high energy". In: *European Physical Journal Web of Conferences*. Vol. 99. European Physical Journal Web of Conferences. Aug. 2015, p. 08001. doi: [10.1051/epjconf/20159908001](https://doi.org/10.1051/epjconf/20159908001) (cited on page 16).
- [77] P. A. M. Dirac. "The Quantum Theory of the Emission and Absorption of Radiation". In: *Proceedings of the Royal Society of London Series A* 114.767 (Mar. 1927), pp. 243–265. doi: [10.1098/rspa.1927.0039](https://doi.org/10.1098/rspa.1927.0039) (cited on page 16).
- [78] I. Esteban et al. "The fate of hints: updated global analysis of three-flavor neutrino oscillations". In: *JHEP* 09 (2020), p. 178. doi: [10.1007/JHEP09\(2020\)178](https://doi.org/10.1007/JHEP09(2020)178) (cited on page 17).

- [79] A. Terliuk. "Measurement of atmospheric neutrino oscillations and search for sterile neutrino mixing with IceCube DeepCore". PhD thesis. Berlin, Germany: Humboldt-Universität zu Berlin, Mathematisch-Naturwissenschaftliche Fakultät, 2018. doi: [10.18452/19304](https://doi.org/10.18452/19304) (cited on page 18).
- [80] J. A. Formaggio and G. P. Zeller. "From eV to EeV: Neutrino cross sections across energy scales". In: *Rev. Mod. Phys.* 84 (3 Sept. 2012), pp. 1307–1341. doi: [10.1103/RevModPhys.84.1307](https://doi.org/10.1103/RevModPhys.84.1307) (cited on page 19).
- [81] L. Fischer. https://github.com/LeanderFischer/icetray_double_cascade_generator_functions (cited on page 23).
- [82] R. Abbasi et al. "LeptonInjector and LeptonWeighter: A neutrino event generator and weighter for neutrino observatories". In: *Comput. Phys. Commun.* 266 (2021), p. 108018. doi: [10.1016/j.cpc.2021.108018](https://doi.org/10.1016/j.cpc.2021.108018) (cited on page 26).
- [83] S. Agostinelli et al. "Geant4—a simulation toolkit". In: *Nucl. Instr. Meth. Phys. Res.* 506.3 (July 2003), pp. 250–303. doi: [10.1016/s0168-9002\(03\)01368-8](https://doi.org/10.1016/s0168-9002(03)01368-8) (cited on pages 26, 34).
- [84] L. Rädel and C. Wiebusch. "Calculation of the Cherenkov light yield from low energetic secondary particles accompanying high-energy muons in ice and water with Geant4 simulations". In: *Astroparticle Physics* 38 (Oct. 2012), pp. 53–67. doi: [10.1016/j.astropartphys.2012.09.008](https://doi.org/10.1016/j.astropartphys.2012.09.008) (cited on pages 26, 34).
- [85] J. Alwall et al. "The automated computation of tree-level and next-to-leading order differential cross sections, and their matching to parton shower simulations". In: *JHEP* 07 (2014), p. 079. doi: [10.1007/JHEP07\(2014\)079](https://doi.org/10.1007/JHEP07(2014)079) (cited on page 27).
- [86] C. Argüelles. <https://github.com/arguelles/NuXSSplMkr> (cited on page 27).
- [87] N. Whitehorn, J. van Santen, and S. Lafebre. "Penalized splines for smooth representation of high-dimensional Monte Carlo datasets". In: *Computer Physics Communications* 184.9 (2013), pp. 2214–2220. doi: <https://doi.org/10.1016/j.cpc.2013.04.008> (cited on page 27).
- [88] J.-M. Levy. "Cross-section and polarization of neutrino-produced tau's made simple". In: *J. Phys. G* 36 (2009), p. 055002. doi: [10.1088/0954-3899/36/5/055002](https://doi.org/10.1088/0954-3899/36/5/055002) (cited on page 27).
- [89] E. Tiesinga et al. "CODATA recommended values of the fundamental physical constants: 2018". In: *Rev. Mod. Phys.* 93 (2 July 2021), p. 025010. doi: [10.1103/RevModPhys.93.025010](https://doi.org/10.1103/RevModPhys.93.025010) (cited on page 29).
- [90] <https://launchpad.net/mg5amcnlo/3.0/3.3.x> (cited on page 30).
- [91] A. Alloul et al. "FeynRules 2.0 - A complete toolbox for tree-level phenomenology". In: *Comput. Phys. Commun.* 185 (2014), pp. 2250–2300. doi: [10.1016/j.cpc.2014.04.012](https://doi.org/10.1016/j.cpc.2014.04.012) (cited on page 30).
- [92] C. Andreopoulos et al. "The GENIE Neutrino Monte Carlo Generator: Physics and User Manual". In: (2015) (cited on page 33).
- [93] M. Glück, E. Reya, and A. Vogt. "Dynamical parton distributions revisited". In: *The European Physical Journal C* 5 (Sept. 1998), pp. 461–470. doi: [10.1007/s100529800978](https://doi.org/10.1007/s100529800978) (cited on page 33).
- [94] A. Bodek and U. K. Yang. "Higher twist, xi(omega) scaling, and effective LO PDFs for lepton scattering in the few GeV region". In: *Journal of Physics G: Nuclear and Particle Physics* 29.8 (2003), p. 1899. doi: [10.1088/0954-3899/29/8/369](https://doi.org/10.1088/0954-3899/29/8/369) (cited on page 33).
- [95] J.-H. Koehne et al. "PROPOSAL: A tool for propagation of charged leptons". In: *Computer Physics Communications* 184.9 (2013), pp. 2070–2090. doi: <https://doi.org/10.1016/j.cpc.2013.04.001> (cited on page 33).
- [96] Y. Becherini et al. "A parameterisation of single and multiple muons in the deep water or ice". In: *Astroparticle Physics* 25.1 (2006), pp. 1–13. doi: <https://doi.org/10.1016/j.astropartphys.2005.10.005> (cited on page 34).
- [97] D. Heck et al. "CORSIKA: A Monte Carlo code to simulate extensive air showers". In: (Feb. 1998) (cited on page 34).
- [98] T. K. Gaisser. "Spectrum of cosmic-ray nucleons, kaon production, and the atmospheric muon charge ratio". In: *Astropart. Phys.* 35 (2012), pp. 801–806. doi: [10.1016/j.astropartphys.2012.02.010](https://doi.org/10.1016/j.astropartphys.2012.02.010) (cited on page 34).

- [99] R. Engel et al. “The hadronic interaction model Sibyll – past, present and future”. In: *EPJ Web Conf.* 145 (2017). Ed. by B. Pattison, p. 08001. doi: [10.1051/epjconf/201614508001](https://doi.org/10.1051/epjconf/201614508001) (cited on page 34).